Available online at www.sciencedirect.com
ScienceDirect
Journal of Sound and Vibration 307 (2007) 393–427
JOURNAL OF SOUND AND VIBRATION
www.elsevier.com/locate/jsvi

Integrated optimization of structural topology and control for piezoelectric smart trusses using genetic algorithm

B. Xu[a,b,*], J.S. Jiang[a], J.P. Ou[b]

[a]*Institute of Vibration Engineering, Department of Engineering Mechanics, Northwestern Polytechnical University, Xi'an 710072, PR China*
[b]*Research Center for Urban & Civil Engineering Disaster Prevention & Reduction, Department of Urban and Civil Engineering, Harbin Institute of Technology Shenzhen Graduate School, Shenzhen 518055, PR China*

Received 28 April 2005; received in revised form 20 April 2007; accepted 5 May 2007

Abstract

In this paper, some issues associated with integrated optimization of structural topology and control for piezoelectric smart trusses are discussed. Based on the optimal coupled control of the modes of piezoelectric smart trusses, the integrated optimization model, including some optimized objective functions, design variables and constraint functions, is built. The design variables include member size, logic design variables of structural topology, the number and placements of actuators/the number of controlled modes as well as the control parameters. Some optimal strategies based on genetic algorithm (GA), such as individual validity examination, structural stability examination and system controllability examination, are adopted to guide the optimization process efficiently. The results of this study show: (1) the optimal topology layout varies with the optimized objective function; (2) the effective damping response time is lowest, if the control index and the damping dissipation velocity index are used as the objective functions for Conditions 1 and 2, respectively; and (3) it is impossible to optimize a objective function under five cases of Condition 1 or 2 simultaneously.

1. Introduction

Up to now, there are commonly and possibly two routes to suppress structural vibration. The first is to execute structural dynamic optimization, including topology optimization, shape optimization as well as size optimization. The theory of size optimization is very much mature and its application is much broad. There are some prodigious developments for shape optimization. Especially, dynamic topology optimization becomes a research emphasis of structural optimization so as to acquire better dynamic characteristics than size optimization and shape optimization for structures [1–5]. The second is to implement passive control, active control or hybrid control. Piezoceramic actuation by the use of smart materials is quite widespread for vibration control. Induced-shear based piezoceramic actuation was applied to reduce helicopter vibration in forward flight by Thakkar et al. [6]. A prototype smart panel with 16 decentralized vibration control units was developed for the reduction of sound radiation/transmission in the theoretic work of Gardonio et al. [7]. The effects of piezoceramic materials on the

*Corresponding author. Tel.: +86 29 8849 2895; fax: +86 29 8849 2216.
E-mail address: xubind@sina.com (B. Xu).

0022-460X/$ - see front matter
doi:10.1016/j.jsv.2007.05.057

active damping of vibrating piezo-composite beams was investigated by Edery-Azulay et al. [8]. A robust H_∞ controller for active structural acoustic control of a smart plate featuring piezoelectric actuators subjected to parameter uncertainties of natural frequency and damping ratio was designed by Choi et al. [9]. Optimization of the placement and feedback gains of an active bar in a closed-loop control system for random intelligent truss structures under stationary random excitation are studied by Gao [10]. The application of piezoceramic actuators in various civil structures such as beams, trusses, steel frames and cable-stayed bridges was reviewed by Song et al. [11]. The effectiveness of linear quadratic regulator (LQR) and linear quadratic Gaussian (LQG) controller to suppress vibrations was investigated for beams with piezoelectric patches acting as sensors or actuators by Vasques et al. [12]. With the development of the application of vibration control, the traditional approach of vibration control is extended from passive control including vibration absorber and the collocation of constraint damping layers to structural optimization. And structural optimization aiming to suppress vibration is also taken as a passive control.

Recently, some attentions are devoted to the integrated optimization of structure and control so as to obtain optimal control effect. Wang et al. [13] presented a new approach for simultaneous optimization of intelligent structures and the control system, where conventional structural sizing variables and elements of the feedback gain matrix are both treated as independent design variables. Fonseca et al. [14] investigated CPU time for solving an integrated structural/control optimization problem of a large space structure with different degrees of freedom. Liu et al. [15,16] presented the optimal control, sensitivity analysis and five algorithms for the integrated optimization of such a multidisciplinary system. Park et al. [17] proposed a preference-based optimization model and applied genetic algorithm (GA) as a numerical search technique for the integrated optimum design of a structural control system. Zhu et al. [18] investigated simultaneous optimization with respect to the structural topology, actuator locations and control parameters of an actively controlled plate structure by a nested solving approach. Xu et al. [19] presented GA to solve the integrated optimization of structure and control for piezoelectric smart trusses with uncertain placement of actuators and sensors, where structural topology and the number of assigned actuators are not dealt with. But above-mentioned researches were confined to an assumption that the number of sensors and actuators is determined in advance. However, further research efforts are required to better solve practical problems for the implementation of controlled systems before widespread application of this novel integrated optimization technology becomes possible. These practical problems include limited number of sensors and controllers, structural topology, and reliability issues, etc. In fact, the number of actuators has significant effects on the control performance of structural response. There were few papers dealing with optimizing the number of piezoelectric actuators under the fixed controlled modes or controlling more modes under the fixed number of actuators. From the view of engineering practice, due to the expensive cost of actuators, it is valuable that how to achieve the optimal control effect with the least number of actuators. Conversely, it is also important to control more modes of the system with the fixed number of actuators to satisfy some control requirements. Therefore, it is necessary to study the control efficiency with a least or limited number of actuators for the integrated optimization. Further, without a doubt, structural topology is also a very sensitive factor, which should be taken into consideration for the integrated optimization.

In order to obtain better control efficiency, two significant and important factors, i.e., structural topology and the number of assigned actuators/the number of controlled modes, are simultaneously taken into account for the integrated optimization in the paper. The article is organized in the following manner. The optimal model, including design variables, objective functions and constraint functions is put forward in Section 2; the corresponding optimization algorithm is discussed in Section 3 and finally, two numerical examples in Section 4 are used to highlight and demonstrate the effectiveness of the proposed method.

2. Optimization problem statement

The present integrated optimization problem is stated as follows:

$$\begin{aligned} &\text{find} && \mathbf{d}_s, \mathbf{d}_c \\ &\min(\text{or } \max) && J(\mathbf{d}_s, \mathbf{d}_c) \\ &\text{s.t.} && \mathbf{g}(\mathbf{d}_s, \mathbf{d}_c)\{\leqslant \text{or } =\}\mathbf{0}, \end{aligned} \tag{1}$$

where $\mathbf{d}_s$ and $\mathbf{d}_c$ are the structural design variable vector and the control design variable vector, respectively; $J(\mathbf{d}_s, \mathbf{d}_c)$ is the optimized objective function. $\mathbf{g}(\mathbf{d}_s, \mathbf{d}_c)$ is the constraint function vector.

2.1. Design variable

The design variable vector is commonly composed of the structural design variable vector and the control design variable vector. The elements of $\mathbf{d}_s$ may be structural size and the logic design variable, which denotes whether there is an element connected to the nodes and deals with the change of structural topology, i.e.,

$$\tilde{\mathbf{A}} = (A_1, \ldots, A_k, \ldots, A_{n_A}), \tag{2}$$

$$\bar{\mathbf{Z}} = (z_1, \ldots, z_k, \ldots, z_{n_A}) \quad \forall z_k \in \{0, 1\}, \tag{3}$$

where A_k is the cross-sectional area of the kth element and n_A is the number of structural elements; when $z_k = 1$, it implies that the corresponding element exists, or else it is removed.

Also, the elements of $\mathbf{d}_c$ may be the feedback gain, the number and placements of actuators/sensors as well as the number of the controlled modes.

2.2. Objective function

2.2.1. Structural mass

In general, we aim to minimize the total mass J_W of the controlled structure, i.e.

$$J_W = \sum_{k=1}^{n_A} \rho_k A_k z_k l_k \to \min, \tag{4}$$

where ρ_k and l_k are the mass density and the length of the kth element, respectively.

2.2.2. Damping dissipation velocity index of system energy

Assuming that the control force vector $\mathbf{u}(t)$ corresponding to Eq. (A.7) in Appendix A can also be written as

$$\mathbf{u}(t) = -\mathbf{G}_1 \dot{\mathbf{y}}_c(t) - \mathbf{G}_2 \mathbf{y}_c(t), \tag{5}$$

where $\mathbf{G}_1$ and $\mathbf{G}_2$ denote the gains associated with modal velocity and modal displacement feedbacks, respectively.

Substituting Eq. (5) into Eq. (A.3) in Appendix A, we have

$$\ddot{\mathbf{y}}_c + \boldsymbol{\varphi}_c^{\mathrm{T}} \mathbf{B} \mathbf{G}_1 \dot{\mathbf{y}}_c + (\boldsymbol{\varphi}_c^{\mathrm{T}} \mathbf{B} \mathbf{G}_2 + \boldsymbol{\Lambda}_c) \mathbf{y}_c = \mathbf{0}. \tag{6}$$

Because an asymmetric matrix can be decomposed into a symmetric (sym) matrix and a skew symmetric (ss) matrix, the modal damping matrix $\boldsymbol{\varphi}_c^{\mathrm{T}} \mathbf{B} \mathbf{G}_1$ of the closed-loop system can be decomposed into two parts, i.e.

$$\mathbf{D}_{\mathrm{sym}} = \tfrac{1}{2}\left(\boldsymbol{\varphi}_c^{\mathrm{T}} \mathbf{B} \mathbf{G}_1 + [\boldsymbol{\varphi}_c^{\mathrm{T}} \mathbf{B} \mathbf{G}_1]^{\mathrm{T}}\right), \tag{7}$$

$$\mathbf{D}_{\mathrm{ss}} = \tfrac{1}{2}\left(\boldsymbol{\varphi}_c^{\mathrm{T}} \mathbf{B} \mathbf{G}_1 - [\boldsymbol{\varphi}_c^{\mathrm{T}} \mathbf{B} \mathbf{G}_1]^{\mathrm{T}}\right). \tag{8}$$

The symmetric part of the modal damping matrix produces the modal damping resistance so that the system energy can be dissipated. However, the skew symmetric part only produces the gyroscopic effect and does not dissipate the system energy. Thus the dissipation energy W_c corresponding to the damping is

$$\mathbf{W}_c = -\frac{1}{2} \int_0^t \dot{\mathbf{y}}_c^{\mathrm{T}} \mathbf{D}_{\mathrm{sym}} \dot{\mathbf{y}}_c \, \mathrm{d}t = \frac{1}{4} \int_0^t \dot{\mathbf{y}}_c^{\mathrm{T}} \left(\boldsymbol{\varphi}_c^{\mathrm{T}} \mathbf{B} \mathbf{G}_1 + [\boldsymbol{\varphi}_c^{\mathrm{T}} \mathbf{B} \mathbf{G}_1]^{\mathrm{T}}\right) \dot{\mathbf{y}}_c \, \mathrm{d}t. \tag{9}$$

Then the dissipation velocity of the system energy is

$$\dot{W}_c = -\tfrac{1}{2} \dot{\mathbf{y}}_c^{\mathrm{T}} \mathbf{D}_{\mathrm{sym}} \dot{\mathbf{y}}_c. \tag{10}$$

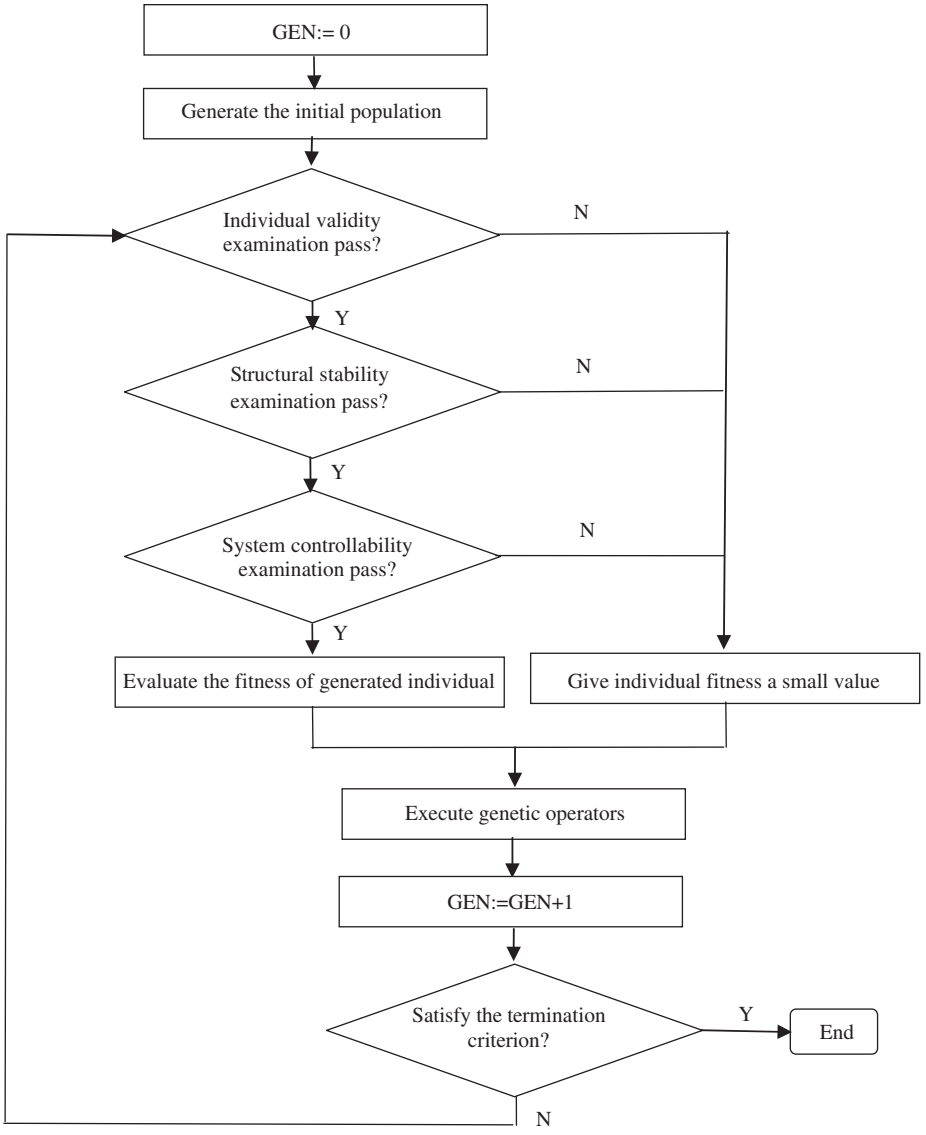

Fig. 1. The flow chart of the optimization algorithm.

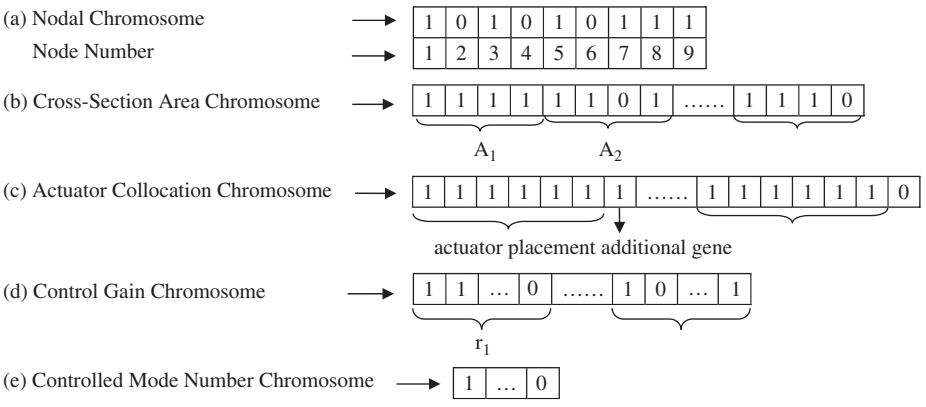

Fig. 2. Chromosome constructions of different design variables.

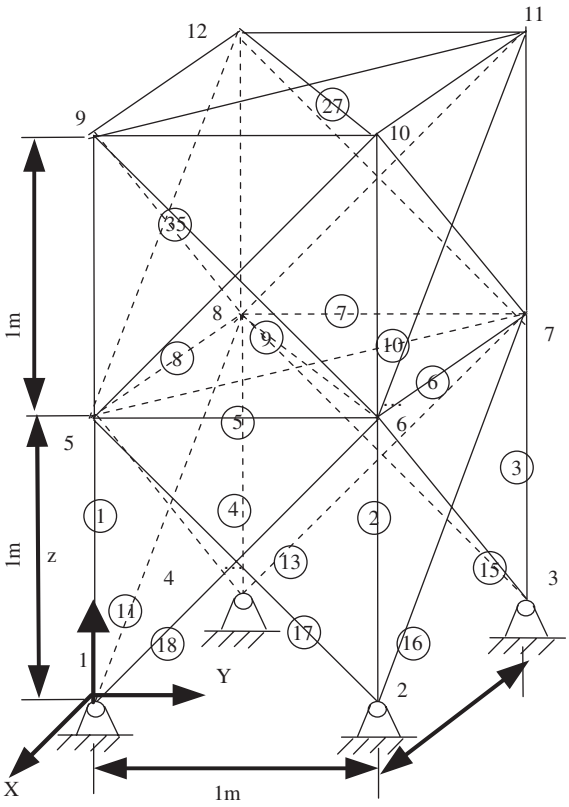

Fig. 3. 36-bar space smart truss.

Table 1
Some parameters of the controlled structure

Mass density of common metal element	2710 kg/m^3
Young's modulus of common metal element	70 GPa
Mass density of connected bar	8000 kg/m^3
Young's modulus of connected bar	210 GPa
Cross-sectional area of connected bar	6.9×10^{-5} m^2
Mass density of piezoelectric stack	7600 kg/m^3
Young's modulus of piezoelectric stack	63 GPa
Cross-sectional area of piezoelectric stack	7.07×10^{-4} m^2
Number of circular piezoelectric patches	490
Thickness of each piezoelectric patch	0.56 mm
Equivalent stress coefficient e_{33}^e	1746 N/(V m)

According to Eq. (10), in order to increase the dissipation velocity, the optimal index can defined as

$$J_c = \mathrm{tr}(\mathbf{D}_{\mathrm{sym}}) = \mathrm{tr}\left(\boldsymbol{\varphi}_c^{\mathrm{T}}\mathbf{B}\mathbf{G}_1 + [\boldsymbol{\varphi}_c^{\mathrm{T}}\mathbf{B}\mathbf{G}_1]^{\mathrm{T}}\right) \to \max \tag{11}$$

where tr( ) denotes the trace of a matrix.

2.2.3. Weighted sum of damping ratios for controlled modes

The pole assignment is to make the poles of the closed-loop system lie left in the complex plane. The complex eigenvalues corresponding to Eq. (A.9) in Appendix A are obtained as

$$\lambda(\bar{\mathbf{A}}) = \bar{\sigma}_i \pm \mathrm{j}\omega_{di}, \quad i = 1, \ldots, n_m, \tag{12}$$

where $\bar{\sigma}_i$ and ω_{di} are the real and image parts of the ith eigenvalue respectively, and $\mathrm{j} = \sqrt{-1}$.

Table 2
Ten optimal solutions of 36-bar space smart truss for Condition 1

	J_W	J_c	J_d	J_{Mc}	J_r
1	120.65	482.64	0.99389	1.1096	0.00027014
2	96.756	456.34	1.0279	1.1724	0.00028794
3	115.36	466.45	0.98413	1.1096	0.00021012
4	126.18	432.67	0.99389	1.1096	0.00018855
5	120.65	466.45	1.0279	1.1724	0.00019851
6	120.65	432.67	0.98413	1.1096	0.00020225
7	102.18	497.86	1.0722	1.1724	0.00026207
8	120.65	527.44	1.5311	1.1096	0.00019851
9	102.18	450.16	1.1911	1.1096	0.00020225
10	120.65	466.45	0.82169	1.1096	0.00019715

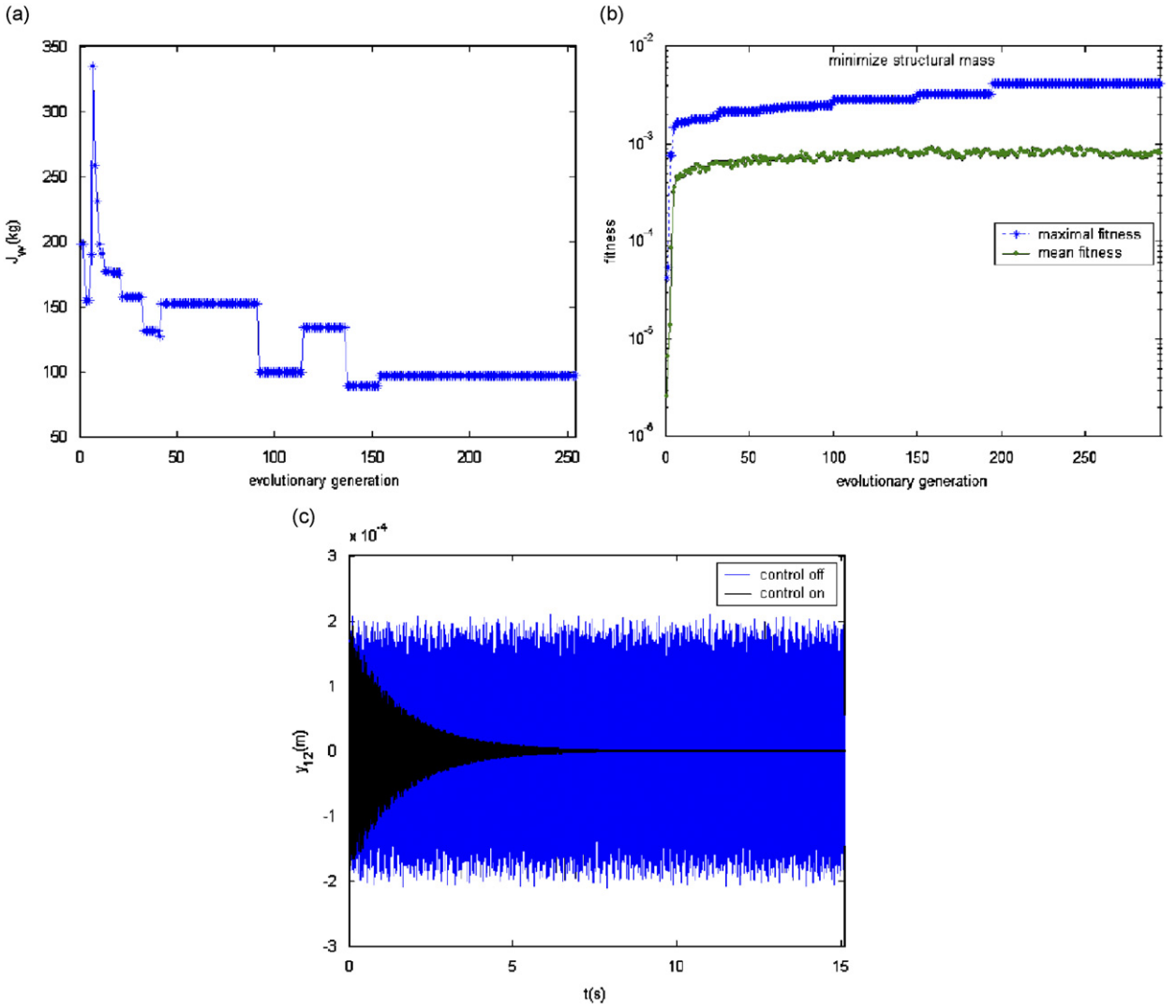

Fig. 4. (a) Curve of structural mass w.r.t. evolutionary generation; (b) curves of the maximal fitness and the mean fitness w.r.t. evolutionary generation; (c) curves of the displacements of node 12 in the y-direction after optimization under two conditions: control off and control on.

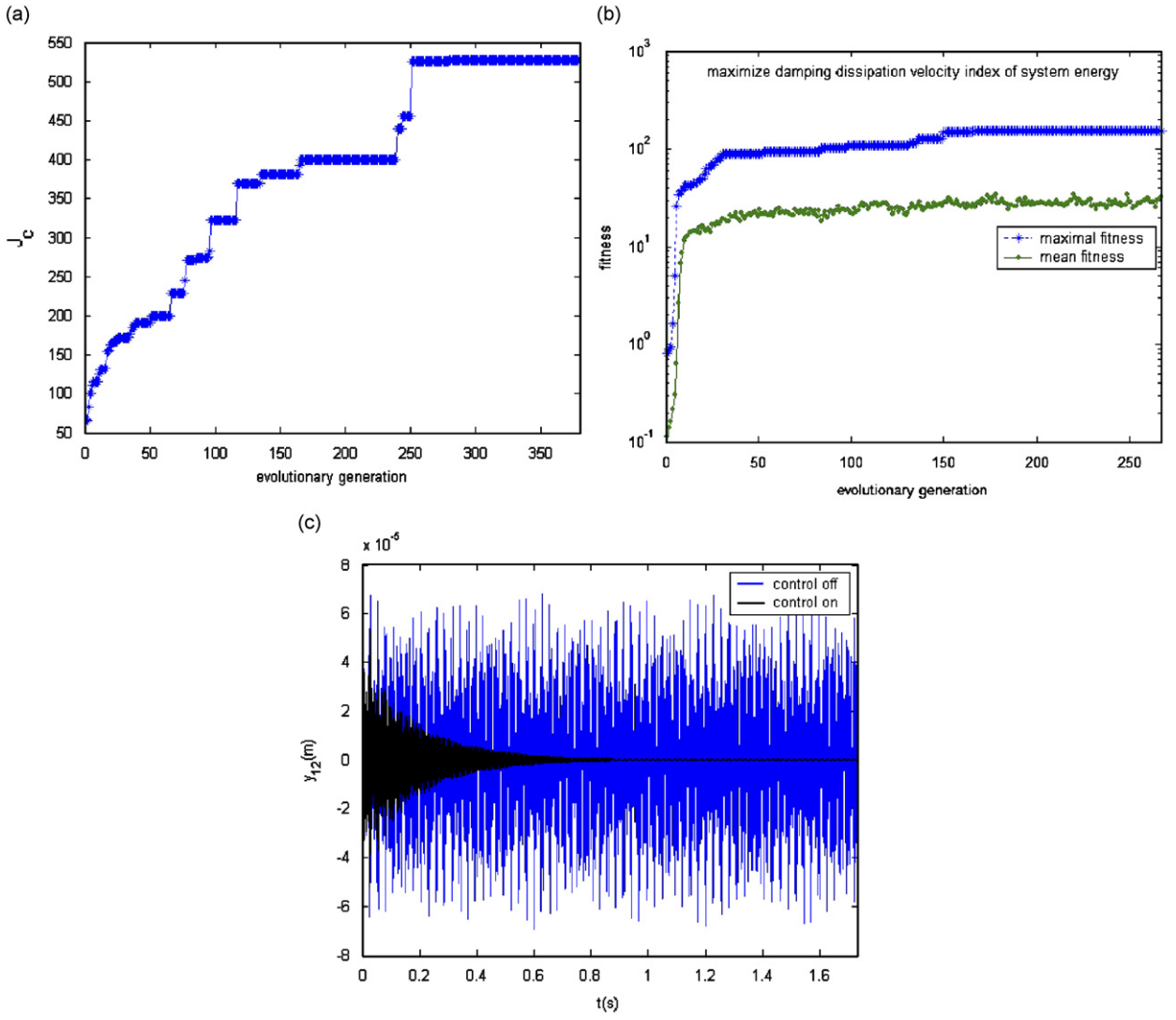

Fig. 5. (a) Curve of the damping dissipation velocity index of system energy w.r.t. evolutionary generation; (b) curves of the maximal fitness and the mean fitness w.r.t. evolutionary generation; (c) curves of the displacements of node 12 in the y-direction after optimization under two conditions: control off and control on.

Based on the complex mode theory, the natural frequency and the damping ratio of the ith complex mode are defined as

$$f_{di} = \omega_{di}/2\pi, \tag{13}$$

$$\xi_i = -\bar{\sigma}_i \Big/ \sqrt{\bar{\sigma}_i^2 + \omega_{di}^2}. \tag{14}$$

If the real part of the eigenvalue of the closed-loop system is larger, i.e., the damp ratio is larger so that the vibration is decayed more quickly and the efficiency of suppressing vibration becomes better. Thus the weighted sum of damping ratios for n_m controlled modes can be considered as an objective function

$$J_d = \sum_{i=1}^{n_m} w_i \xi_i \to \max, \tag{15}$$

where w_i is the weighting factor associated with the ith controlled mode.

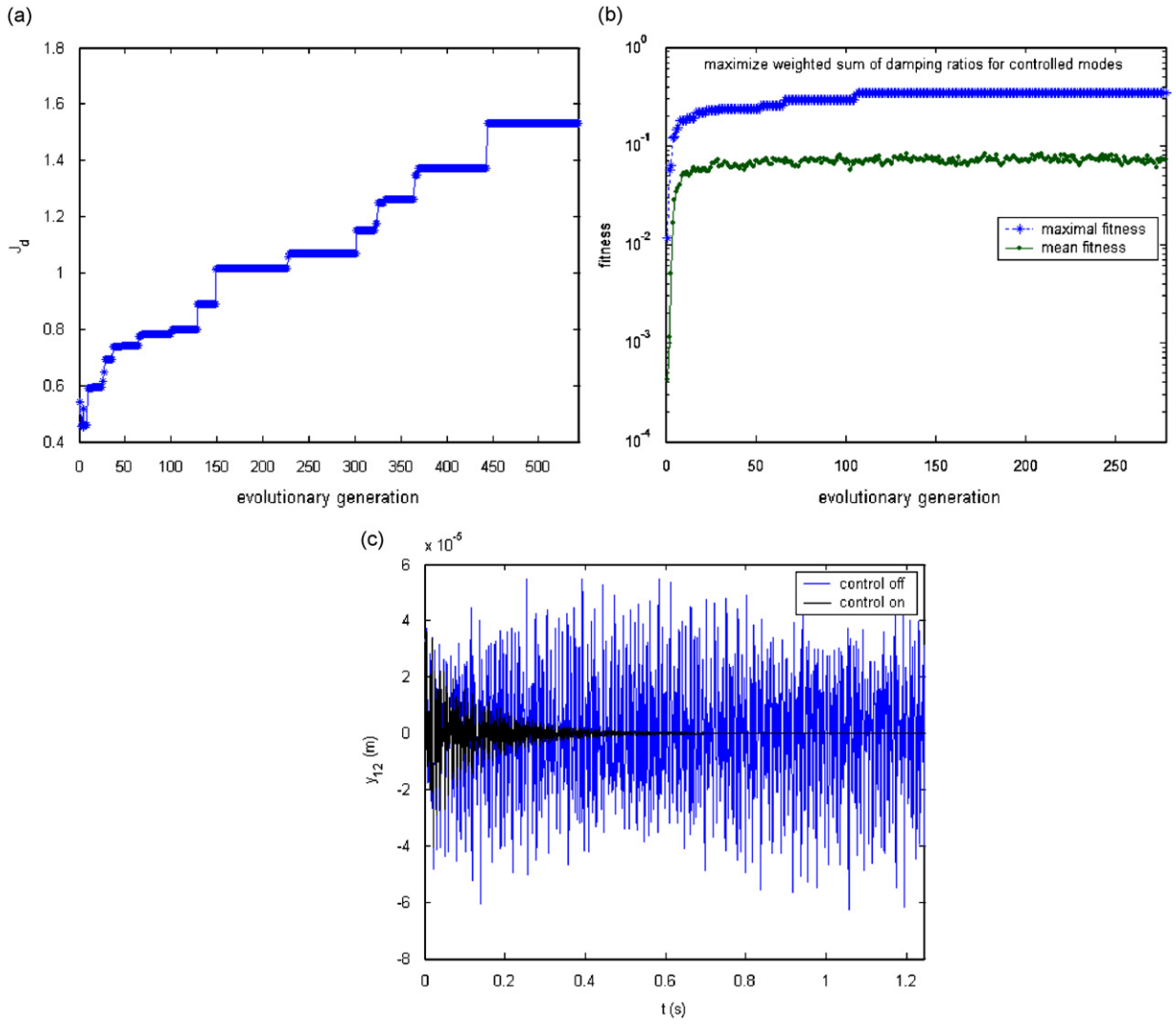

Fig. 6. (a) Curve of the weighted sum of damping ratios for controlled modes w.r.t. evolutionary generation; (b) curves of the maximal fitness and the mean fitness w.r.t. evolutionary generation; (c) curves of the displacements of node 12 in the y-direction after optimization under two conditions: control off and control on.

Since the dynamic response of engineering structures is generally dominated by the first few lower modes, the reasonable weighting factor w_i can be taken as

$$w_i = \frac{1}{\omega_{di}^2} \Big/ \sum_{i=1}^{n_m} \frac{1}{\omega_{di}^2}. \tag{16}$$

2.2.4. Controllability index

The system controllability is commonly taken as one of design criterions for the smart structures and is evaluated by Σ, the singular value of $\mathbf{B}'$ (Eq. (A.3) in Appendix A). The singular value decomposition (SVD) of $\mathbf{B}'$ is expressed as

$$\mathbf{B}' = \mathbf{U}_c \mathbf{S}_C \mathbf{V}_c^{\mathrm{T}}, \tag{17}$$

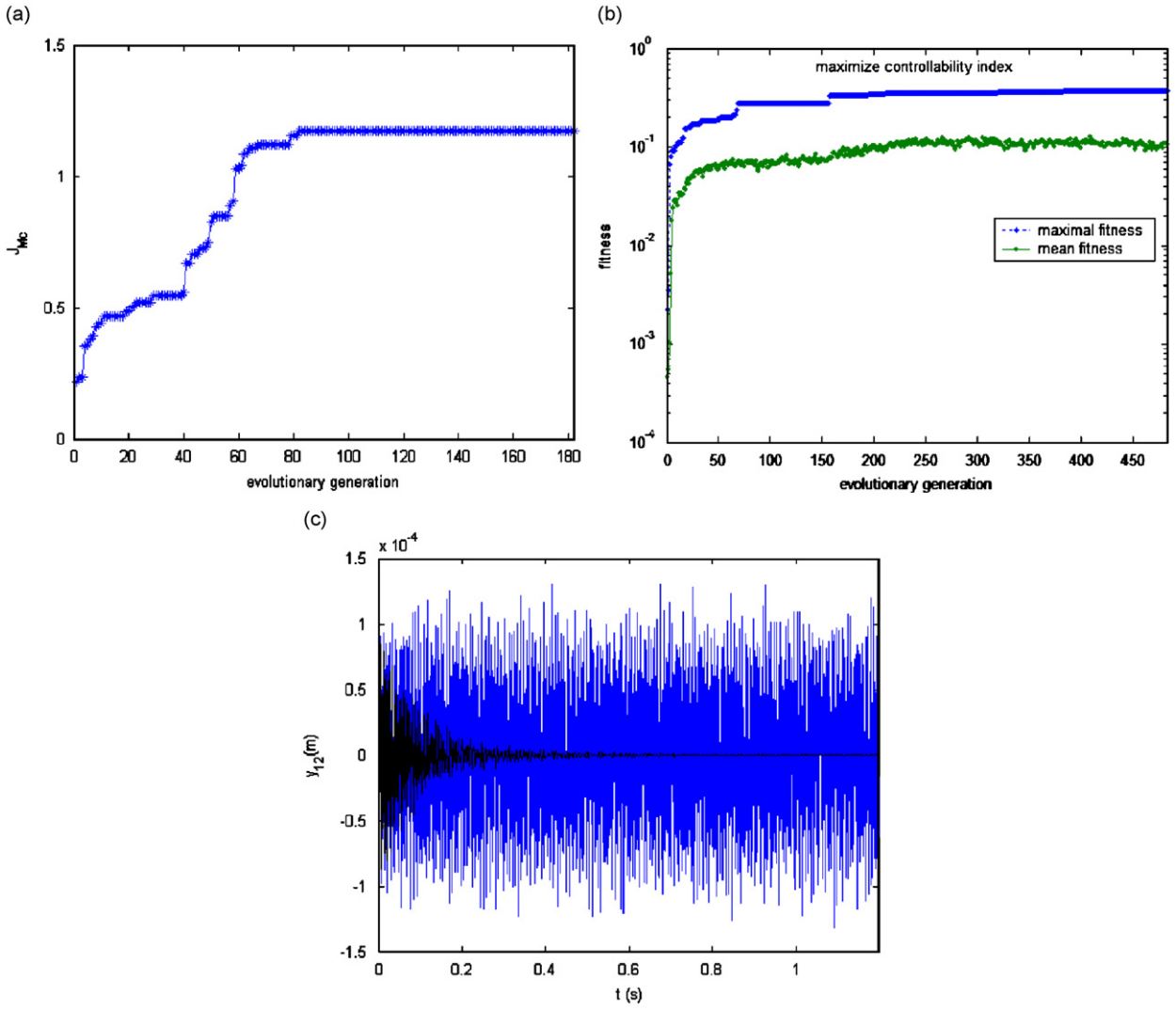

Fig. 7. (a) Curve of controllability index w.r.t. evolutionary generation; (b) curves of the maximal fitness and the mean fitness w.r.t. evolutionary generation; (c) curves of the displacements of node 12 in the y-direction after optimization under two conditions: control off and control on.

where

$$\mathbf{U}_c^{\mathrm{T}}\mathbf{U}_c = \mathbf{I}, \quad \mathbf{V}_c^{\mathrm{T}}\mathbf{V}_c = \mathbf{I} \text{ and } \mathbf{S}_c = \begin{bmatrix} \Sigma & \mathbf{0} \\ \mathbf{0} & \mathbf{0} \end{bmatrix} = \begin{bmatrix} \mathrm{diag}(\tilde{\sigma}_i) & \mathbf{0} \\ \mathbf{0} & \mathbf{0} \end{bmatrix},$$

$\tilde{\sigma}_i (i = 1, 2, \ldots, r)$ is the ith nonzero singular value.

Assume

$$M_c = \|\Sigma\|_E, \tag{18}$$

where $\| \ \|_E$ denotes the Euclidean Norm of a matrix.

If M_c is larger, the required control force is smaller. Then, the optimal index for system controllability can be written as

$$J_{M_c} = M_c = \|\Sigma\|_E \to \max. \tag{19}$$

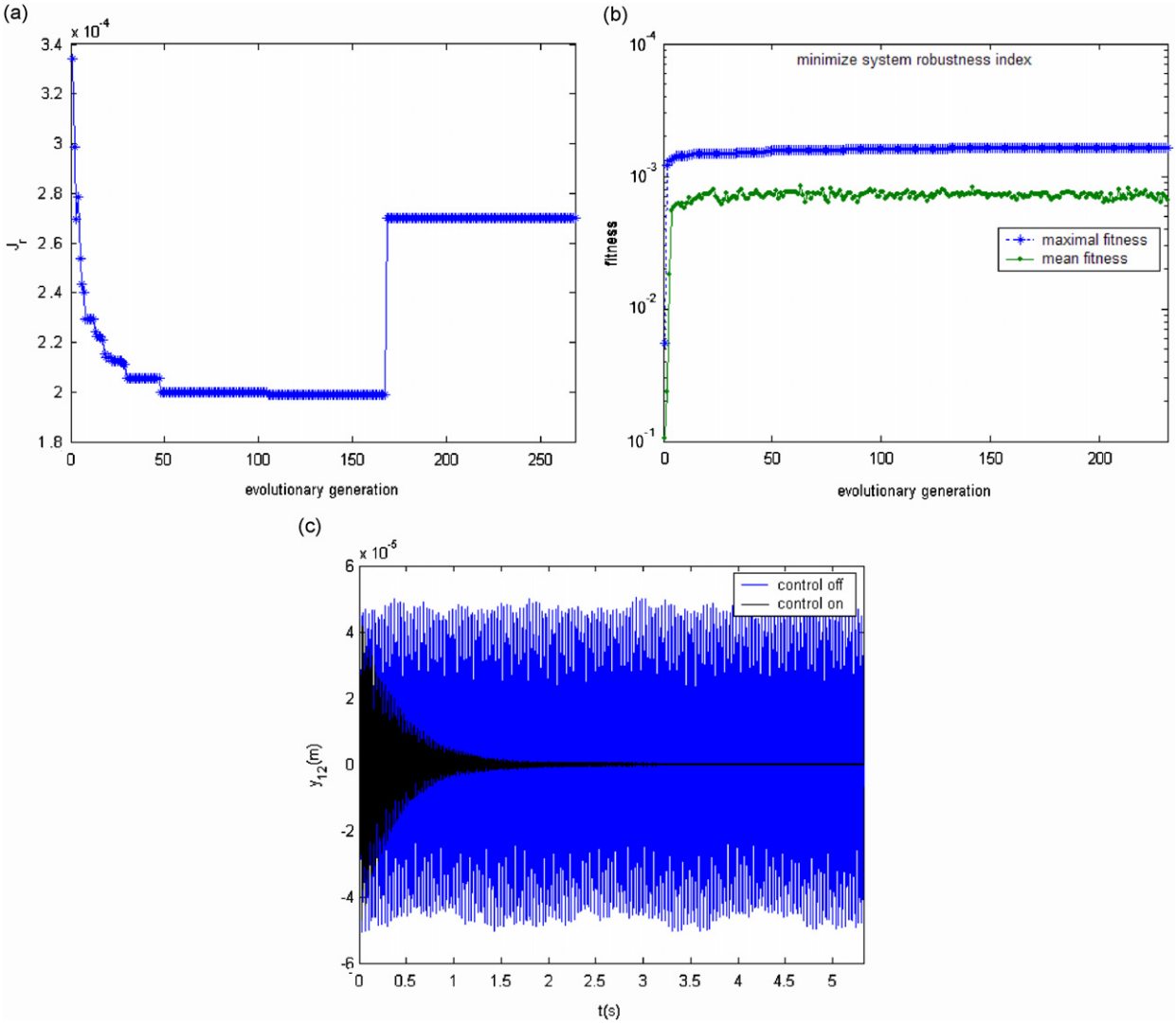

Fig. 8. (a) Curve of system robustness index w.r.t. evolutionary generation; (b) curves of the maximal fitness and the mean fitness w.r.t. evolutionary generation; (c) curves of the displacements of node 12 in the y-direction after optimization under two conditions: control off and control on.

Table 3
Optimal characteristics of 36-bar space smart truss for Condition 1

	σ_{max} (MPa)	f_1 (Hz)	V_{1max} (V)	V_{2max} (V)	V_{3max} (V)	Objective function
Case 1	70.007	107.46	120.05	146.33		96.756
Case 2	11.524	125.04	62.593	107.43	51.454	527.44
Case 3	25.154	100.41	134.86	4.4705	79.678	1.5311
Case 4	11.349	107.31	90.081	87.871	40.106	1.1724
Case 5	51.052	121.25	80.796	134		0.00027

2.2.5. *Robustness index*

In general, the control design deals with the determinate structure. However, the actual dynamic characteristics of the closed-loop system do not depend entirely on the fixed control design. Some unconsidered and uncertain factors may worse the performances of the closed-loop system. Further, it is

Table 4
Optimal design variables of 36-bar space smart truss for Condition 1

Design variable	Case 1	Case 2	Case 3	Case 4	Case 5
A_1	320	1620	1125	1280	3125
A_2	1280	1280	793.8	3125	672.2
A_3	80	1125	1280	259.2	1280
A_4	1620	2420	2000	2420	2000
A_5	180	1125	320	3125	80
A_6	1125	2420	500	80	80
A_7	0	1620	180	125	500
A_8	793.8	3125	1280	1280	@
A_9	1280	259.2	259.2	793.8	320
A_{10}	125	1125	2000	405	500
A_{11}	180	2000	3125	405	672.2
A_{12}	1280	2420	3125	1280	793.8
A_{13}	259.2	180	80	320	1280
A_{14}	@	2000	1620	500	320
A_{15}	0	1280	259.2	@	2420
A_{16}	405	2420	793.8	0	2420
A_{17}	@	672.2	1620	1125	672.2
A_{18}	320	259.2	2420	320	12802
A_{19}	0	1620	259.2	0	3125
A_{20}	259.2	80	0	80	0
A_{21}	0	0	0	0	1280
A_{22}	672.2	672.2	@	793.8	2000
A_{23}	0	0	0	0	0
A_{24}	0	0	0	0	0
A_{25}	0	0	1250	0	1125
A_{26}	0	80	80	0	500
A_{27}	405	@	0	@	0
A_{28}	0	0	@	0	125
A_{29}	793.8	672.2	793.8	1280	793.8
A_{30}	0	793.8	1620	0	672.2
A_{31}	0	0	80	0	@
A_{32}	259.2	125	125	80	405
A_{33}	1280	80	0	@	0
A_{34}	0	0	125	0	1620
A_{35}	0	@	@	0	2000
A_{36}	125	@	0	80	0
$r_1(\times 10^{-3})$	0.9323	0.4621	0.1308	0.7820	0.8963
$r_2(\times 10^{-3})$	0.8550	0.1053	0.9596	0.9974	0.8102
$r_3(\times 10^{-3})$		0.3118	0.3505	0.5948	

Note: @ denotes actuator.

necessary to enlarge the ability of the closed-loop system in order to maintain the predetermined performance index and infinitesimal sensitivity under some uncertain factors, i.e., to aggrandize the robustness of the closed-loop system.

The disturbed closed-loop system corresponding to Eq. (A.9) in Appendix A can be written as

$$\dot{\mathbf{Z}}(t) = (\bar{\mathbf{A}} + \mathbf{\Xi})\mathbf{Z}(t), \tag{20}$$

where $\bar{\mathbf{A}}$ and $\mathbf{\Xi}$ are the steady matrix and the disturbed matrix, respectively.

If the system after disturbance is steady, it must satisfy the following condition:

$$\Xi_{ij} \leqslant \frac{1}{\sup\limits_{P \geqslant 0} \rho\left[\left|(jP^{\#}\mathbf{I} - \bar{\mathbf{A}})^{-1}\right|\mathbf{U}_e\right]} U_{e_{ij}} = \frac{1}{\rho_s} U_{e_{ij}} \tag{21}$$

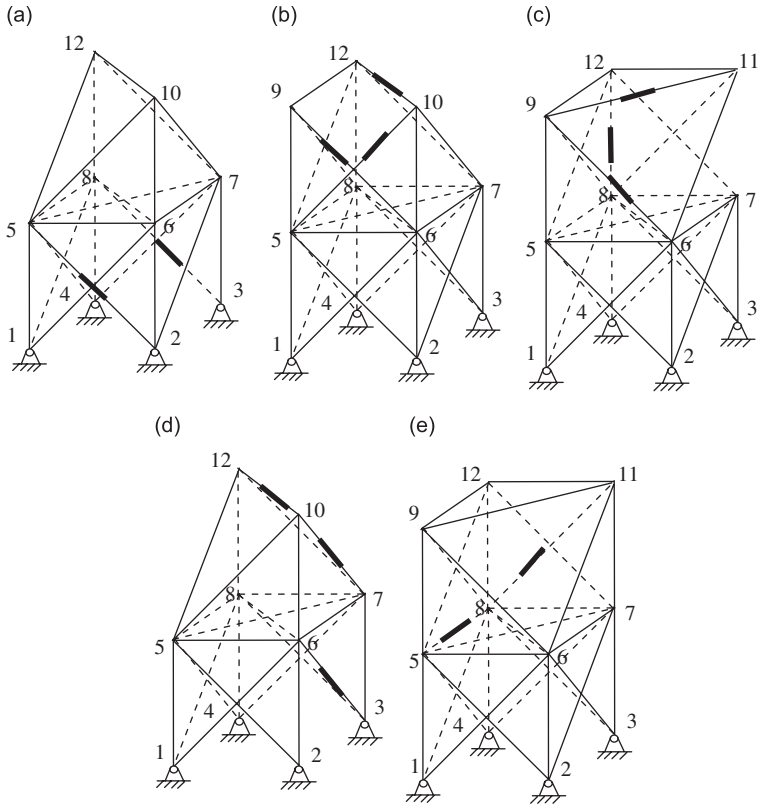

Fig. 9. Optimal topology layouts for Condition 1: (a) minimizing structural mass; (b) maximizing the damping dissipation velocity index of system energy; (c) maximizing the weighted sum of damping ratios for controlled modes; (d) maximizing controllability index; (e) minimizing system robustness index.

Table 5
Optimal characteristics of 36-bar space smart truss for Condition 2

	$\sigma_{\max}$ (MPa)	f_1 (Hz)	$V_{1\max}$ (V)	$V_{2\max}$ (V)	n_m	Objective function
Case 1	11.426	92.5604	114.4656	70.4202	4	46.9357
Case 2	13.437	116.4921	47.7237	68.7403	4	1142.8
Case 3	23.683	90.7936	138.1302	74.0364	3	7.4281
Case 4	15.998	85.6814	63.7904	36.1597	4	0.8270
Case 5	25.617	100.5462	81.8777	67.9842	5	0.00037489

where $|\ |$ denotes the absolute value; $\rho[\ ]$ is the spectral radius of a matrix; sup is the supremum of the matrix within the range of $P^{\#}$ (the frequency of the excited force); $U_{e_{ij}}$ is the element of the disturbed discriminating matrix $\mathbf{U}_e$ and its value lies between 0 and 1. If any element of the matrix $\bar{\mathbf{A}}$ is a constant or zero, any element of $\mathbf{U}_e$ is zero and there is no disturbance for the system.

In order to obtain the performance index of system robustness, it is necessary to calculate the ρ_s in Eq. (21). The spectral radius is the maximal eigenvalue of the matrix $|(\mathrm{j}P^{\#}\mathbf{I}-\bar{\mathbf{A}})^{-1}|\mathbf{U}_e$ when the operational frequency $P^{\#}$ equals to a certain value. Then the corresponding critical operator frequency is defined as $P^{\#}_{\mathrm{cr}}$. The peak value of the spectral radius equals to the spectral radius of the matrix $|(\mathrm{j}P^{\#}_{\mathrm{cr}}\mathbf{I}-\bar{\mathbf{A}})^{-1}|\mathbf{U}_e$ only when $P^{\#}$ is the module of eigenvalue of the closed-loop system. Therefore, for the appointed critical operator frequency $P^{\#}_{\mathrm{cr}}$, the maximal eigenvalue of the matrix $|(\mathrm{j}P^{\#}_{\mathrm{cr}}\mathbf{I}-\bar{\mathbf{A}})^{-1}|\mathbf{U}_e$ is

$$\tilde{\lambda}_\rho = \tilde{\lambda}^r_\rho + \mathrm{j}\tilde{\lambda}^i_\rho, \tag{22}$$

where $\tilde{\lambda}^r_\rho$ and $\tilde{\lambda}^i_\rho$ are the real part and the image part of $\tilde{\lambda}_\rho$, respectively.

Table 6
Optimal design variables of 36-bar space smart truss for Condition 2

Design variable	Case 1	Case 2	Case 3	Case 4	Case 5
A_1	1125	3125	3125	3125	2000
A_2	259.2	1620	3125	500	3125
A_3	320	405	1280	3125	2000
A_4	1620	3125	3125	3125	2420
A_5	80	259.2	500	1620	259.2
A_6	180	793.8	125	80	1280
A_7	80	2420	259.2	125	500
A_8	0	500	125	3125	@
A_9	0	80	259.2	1280	2420
A_{10}	80	320	125	2000	320
A_{11}	125	2000	1280	3125	2420
A_{12}	672.2	3125	2420	2420	3125
A_{13}	80	125	405	500	@
A_{14}	125	500	80	@	320
A_{15}	500	405	500	1280	1125
A_{16}	0	500	180	405	1280
A_{17}	80	405	1620	259.2	80
A_{18}	@	672.2	180	80	500
A_{19}	0	0	80	1620	0
A_{20}	0	405	0	80	1620
A_{21}	@	80	125	0	672.2
A_{22}	320	125	500	0	793.8
A_{23}	0	0	0	0	0
A_{24}	0	125	0	0	80
A_{25}	180	@	80	0	0
A_{26}	0	0	0	259.2	0
A_{27}	0	0	0	@	0
A_{28}	0	0	@	0	0
A_{29}	320	125	672.2	80	180
A_{30}	0	0	405	1620	0
A_{31}	125	80	259.2	0	125
A_{32}	0	0	180	0	80
A_{33}	0	@	0	80	259.2
A_{34}	125	0	0	0	793.8
A_{35}	0	0	@	125	0
A_{36}	0	1125	0	80	125
$r_1(\times 10^{-4})$	0.4384	0.1000	0.1193	0.6704	0.5061
$r_2(\times 10^{-4})$	0.5641	0.1483	0.4287	0.6027	0.6994

Then

$$\rho_s = \left[(\tilde{\lambda}_\rho^r)^2 + (\tilde{\lambda}_\rho^i)^2\right]^{1/2}. \tag{23}$$

Correspondingly, the optimized performance index for system robustness is defined as

$$J_r = \rho_s \to \min, \tag{24}$$

where when J_r becomes smaller, the robustness of the closed-loop system become stronger.

2.3. Constraint function

The constraints include not only the constraints for the structural system but also the constraints for the control system. In order to work better, engineering structures should satisfy the dynamic design condition as well as the static design condition, i.e., the elements of the controlled structures should satisfy the stress and

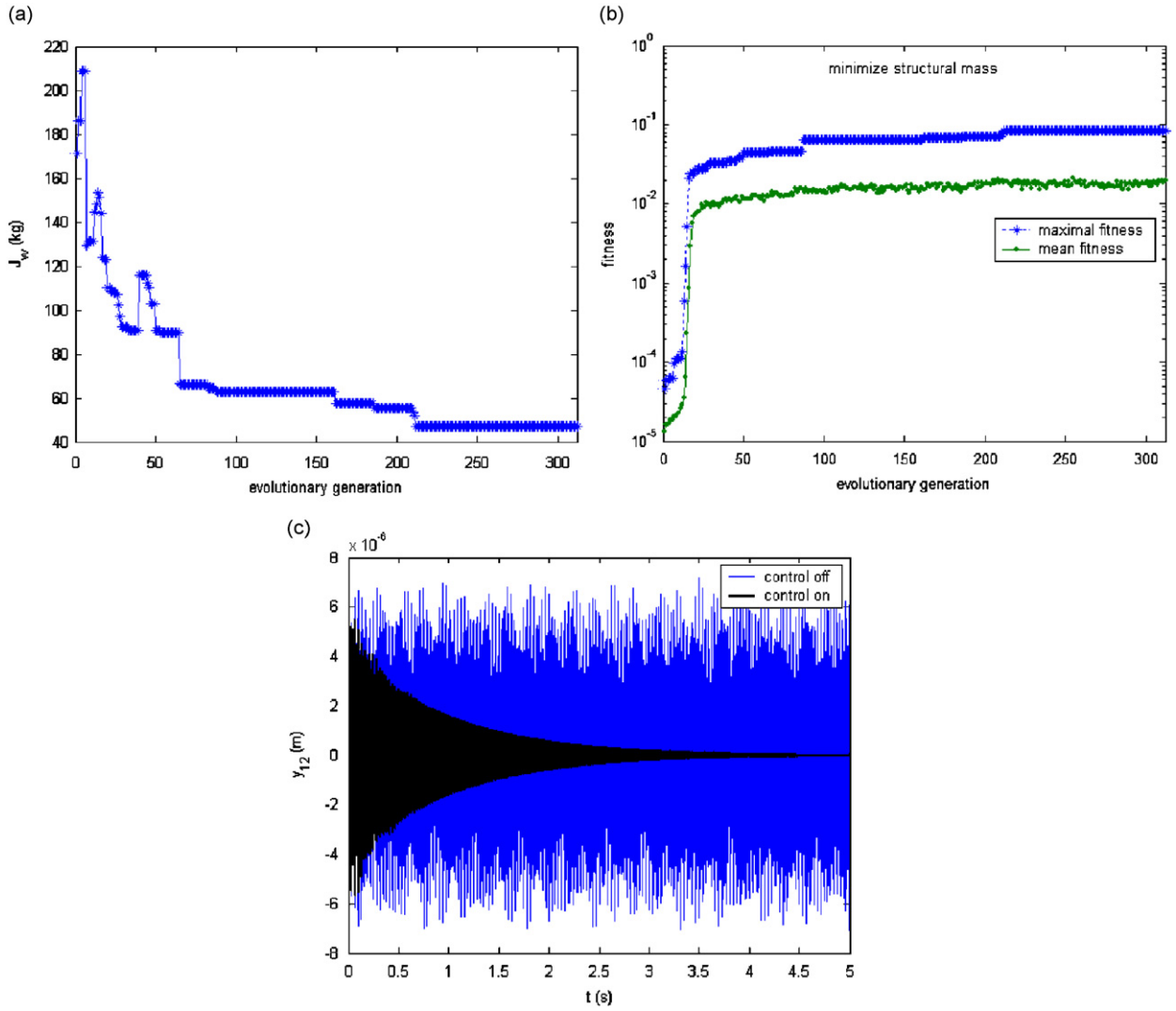

Fig. 10. (a) Curve of structural mass w.r.t. evolutionary generation; (b) curves of the maximal fitness and the mean fitness w.r.t. evolutionary generation; (c) curves of the displacements of node 12 in the y-direction after optimization under two conditions: control off and control on.

nodal displacement requirements under static condition. These conditions can be written as

$$\sigma_k^u - z_k\sigma_k \geqslant 0 \quad \forall k = 1, \ldots, n_A, \tag{25}$$

$$\delta_{jl}^u - \gamma_j\delta_{jl} \geqslant 0, \tag{26}$$

$$\gamma_j \in \{0, 1\} = \begin{cases} 0 & \text{when node } j \text{ is removed,} \\ 1 & \text{when node } j \text{ exists,} \end{cases} \tag{27}$$

where σ_k and σ_k^u are the stress and the corresponding upper bound of the kth element, respectively; δ_{jl} and δ_{jl}^u are the displacement and the corresponding upper bound of the jth node along the lth direction, respectively. In engineering practice, in order to ensure the dynamic characteristics, and avoid the resonance or the coupled effect between the structure and the external excitation, it is common to impose the constraint on the rth natural frequencies of the optimized structure, especially for the first natural frequency. Accordingly, its

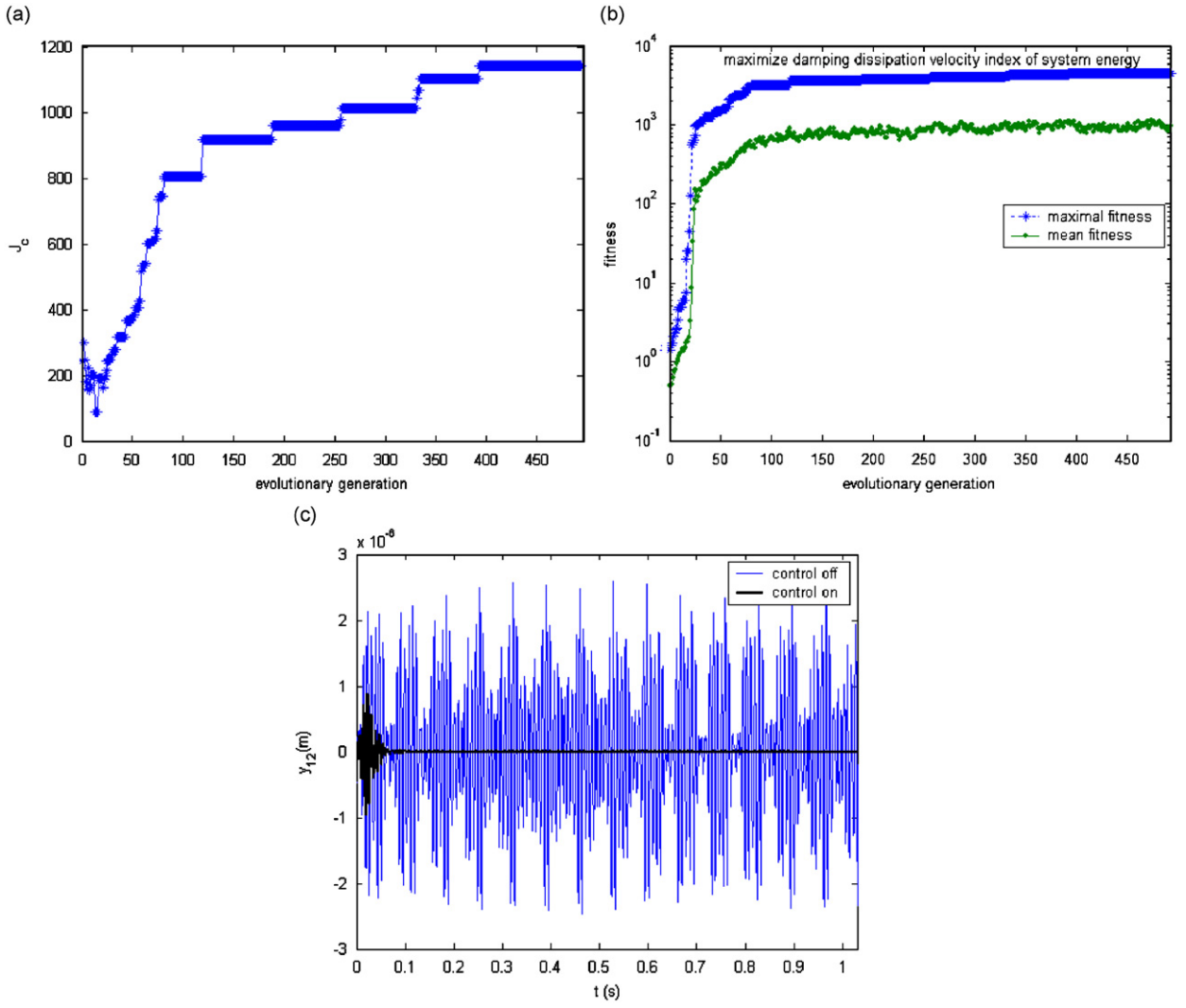

Fig. 11. (a) Curve of the damping dissipation velocity index of system energy w.r.t. evolutionary generation; (b) curves of the maximal fitness and the mean fitness w.r.t. evolutionary generation; (c) curves of the displacements of node 12 in the y-direction after optimization under two conditions: control off and control on.

expression may be one of three cases:

$$f_r \leqslant f_r^u, \tag{28}$$

$$f_r^l \leqslant f_r, \tag{29}$$

$$f_r^l \leqslant f_r \leqslant f_r^u, \tag{30}$$

where f_r is the rth natural frequency of the open-loop system, f_r^u and f_r^l are the corresponding upper and low bounds, respectively.

Because there is a break-over voltage for the piezoelectric patches and the applied voltage by the voltage amplifier is limited also, the active control system cannot provide the unlimited and necessary control force beyond the break-over voltage. Then the constraint on the active control force can be transformed as the corresponding voltage constraint, i.e.,

$$V_m^u - V_m \geqslant 0 \quad \forall m = 1, \ldots, n_a, \tag{31}$$

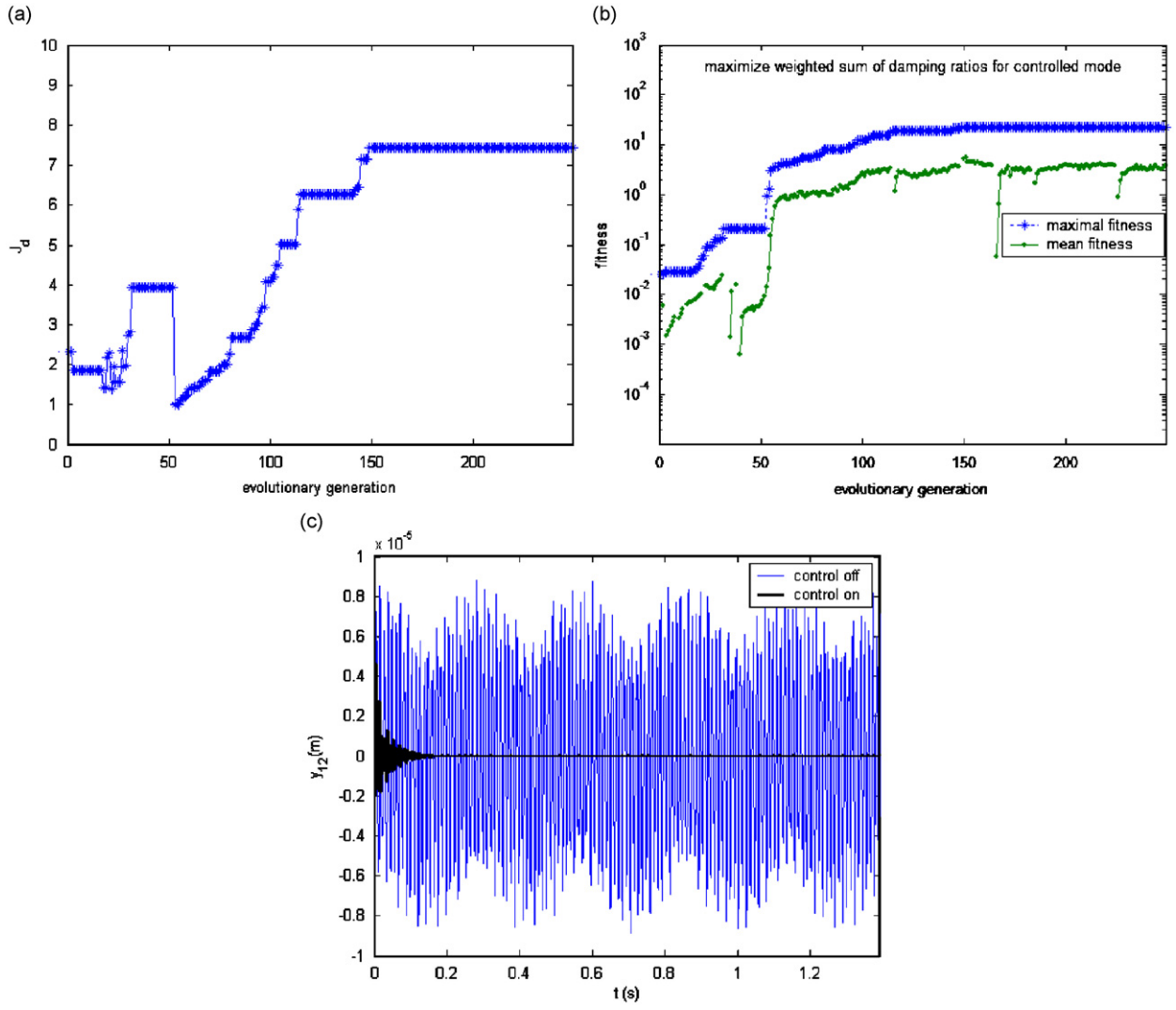

Fig. 12. (a) Curve of the weighted sum of damping ratios for controlled modes w.r.t. evolutionary generation; (b) curves of the maximal fitness and the mean fitness w.r.t. evolutionary generation; (c) curves of the displacements of node 12 in the y-direction after optimization under two conditions: control off and control on.

where V_m and V_m^u are the applied voltage and the corresponding upper bound of the mth actuator, respectively. Here, the diagonal elements r_m of $\mathbf{R}$ (Eq. (A.6) in Appendix A) is taken as the design variables for the control design and should be confined to a specified range, i.e.,

$$r_m^l \leqslant r_m \leqslant r_m^u \quad \forall m = 1, \ldots, n_a, \tag{32}$$

where r_m is the mth controller gain; r_m^u and r_m^l are the corresponding upper and low bounds, respectively.

3. Optimization algorithm

Because the design variable space is composed of two different types of design variables: discrete and continuous, and the change of structural topology may lead to the singular phenomenon, some optimization

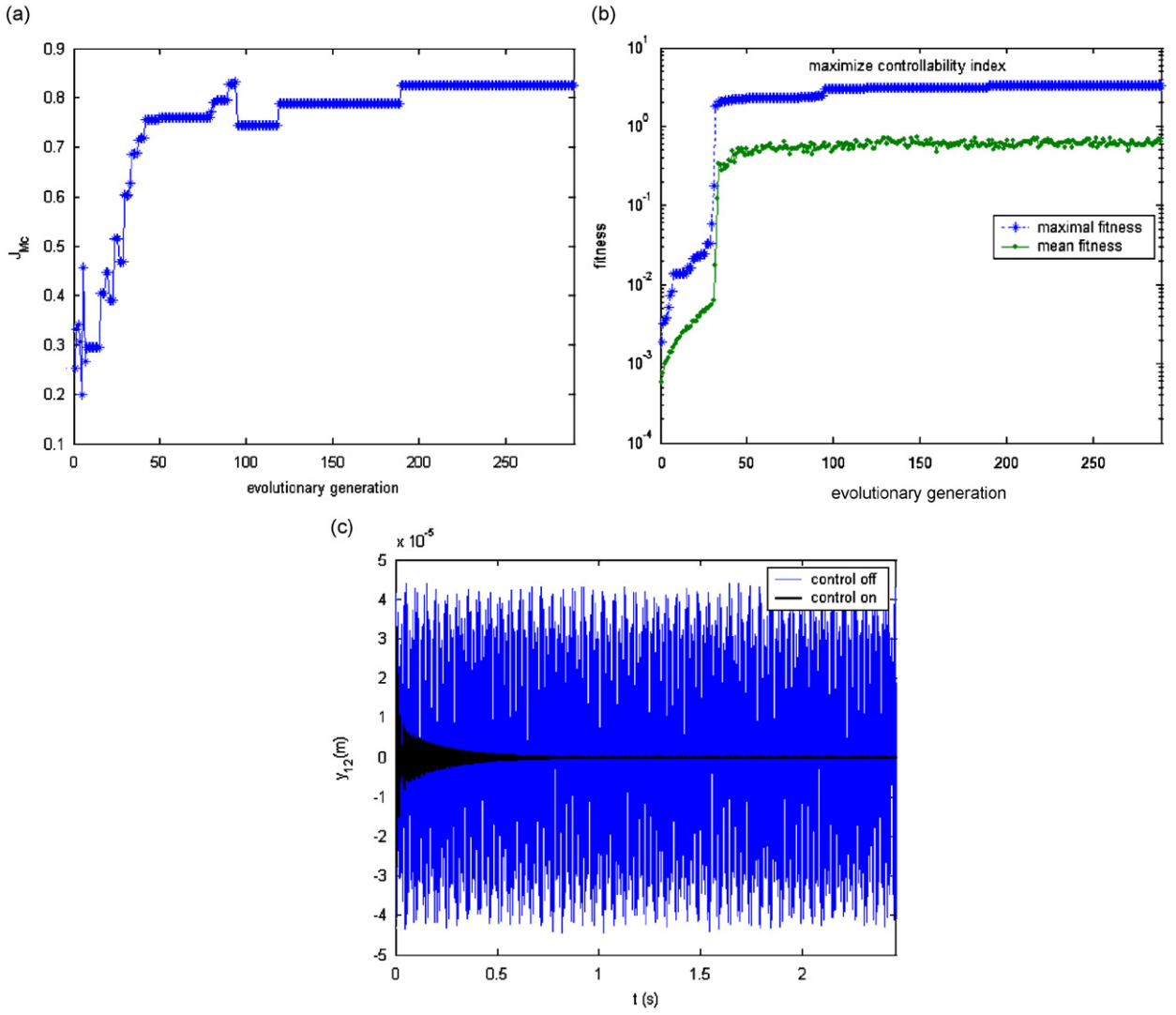

Fig. 13. (a) Curve of controllability index w.r.t. evolutionary generation; (b) curves of the maximal fitness and the mean fitness w.r.t. evolutionary generation; (c) curves of the displacements of node 12 in the y-direction after optimization under two conditions: control off and control on.

strategies are adopted to guide the integrated optimization of structural topology and control efficiently. The flow chart of the optimization algorithm is shown in Fig. 1. Some basic ideals are explained as follows:

1. *Code*: The decimal value of each design variable is encoded into a gene represented by binary code. Accordingly, the chromosome constructions of different kinds of design variables are shown in Fig. 2. In order to speed up the optimal process, nodal information besides the support nodes and the node on which external loads are imposed is also coded into a chromosome, where a value of 1 assigned to a node corresponds to the presence of a node and a value 0 to a removed node. When a node is removed, the cross-sectional areas of all elements connected to such node are zeroes. For the problem to optimize the number of piezoelectric actuators, an additional gene is used to account for whether the actuator is placed. If the gene value is 1, an actuator is placed on the corresponding location. Or else, it is not placed. Then all corresponding chromosomes are joined together to represent a design variable vector.

2. *Individual validity examination*: The ''individual validity examination'' is performed by examining whether the individual code is effective. Commonly, there are redundant codes for the design variables. If the coding of

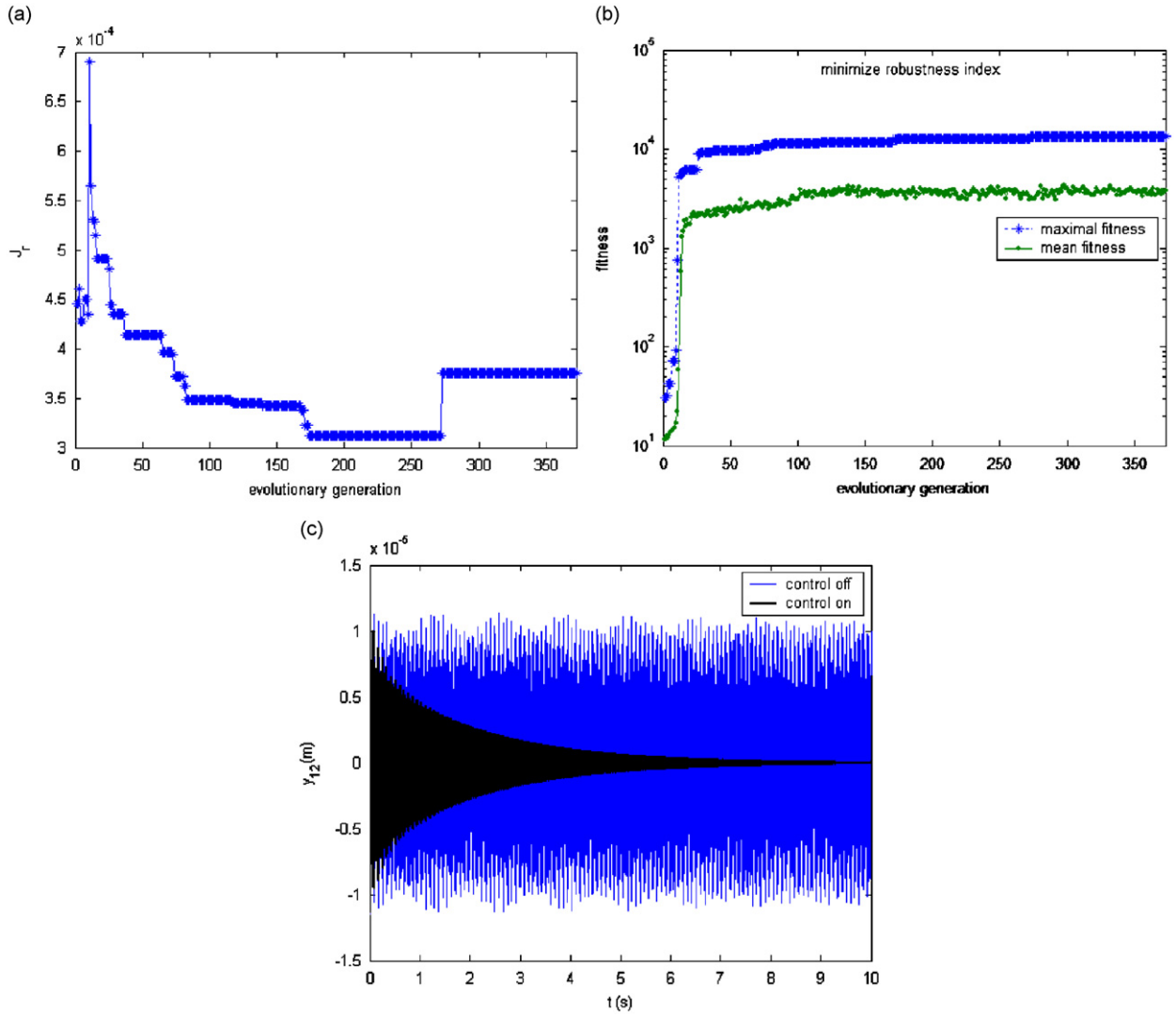

Fig. 14. (a) Curve of system robustness index w.r.t. evolutionary generation; (b) curves of the maximal fitness and the mean fitness w.r.t. evolutionary generation; (c) curves of the displacements of node 12 in the y-direction after optimization under two conditions: control off and control on.

a certain design variable of a design variable vector is meaningless, the corresponding individual is meaningless and need not be analyzed any further.

3. *Structural stability examination*: The ''structural stability examination'' is performed by two steps, i.e., ''nodal examination'' and ''rigid body movement examination''. The ''nodal examination'' is performed by examining whether there is a node, which is only connected to two members. This is because when a node with no external loads to which is only connected by two members, which do not lie along with a straight line, the node must be meaningless, as those two members will not bear any stress. Therefore, when a topology has at least one such node, the topology can then be taken as meaningless one and it is certainly unnecessary to do any further optimization analysis. The ''rigid body movement examination'' is performed by examining whether the stiffness matrix is singular. Although all nodes of a certain topology are meaningful, the corresponding structure can still be a mechanism that results in rigid body movement. When a topology creates rigid body movement, it must be unable to bear some types of external loads. Thus, it is meaningless and need not be analyzed any further too.

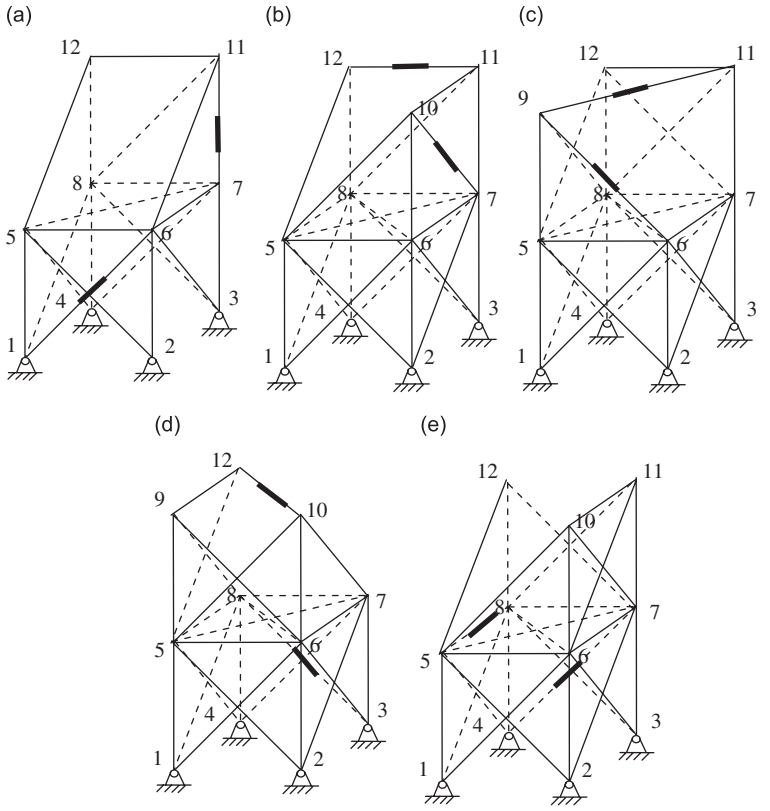

Fig. 15. Optimal topology layouts for Condition 2: (a) minimizing structural mass; (b) maximizing the damping dissipation velocity index of system energy; (c) maximizing the weighted sum of damping ratios for controlled modes; (d) maximizing controllability index; (e) minimizing system robustness index.

4. *System controllability examination*: The "system controllability examination" is performed by examining whether Eq. (A.5) in the Appendix A is tenable. In order to ensure system controllability, if the actuator assignment does not satisfy Eq. (A.5), the controlled structure need not be analyzed any further too.

5. *Evaluation of individual fitness*: An optimization problem is transformed into an unconstrained optimization problem by Penalty Function Method. For GA, the individual fitness is formed by the objective function and the penalty function. A design variable vector with invalid string is invalid too. Accordingly, its fitness can be given a small value, i.e.

$$\text{eval}(\mathbf{d}_s, \mathbf{d}_c) = \varepsilon_1 \quad \text{invalid individual}, \tag{33}$$

where ε_1 is a prescribed small value.

Furthermore, if the system is unstable or uncontrollable, its corresponding fitness should also be given a small value, i.e.,

$$\text{eval}(\mathbf{d}_s, \mathbf{d}_c) = \varepsilon_1 \quad \text{unstable or uncontrolled system}. \tag{34}$$

Define the degree of constraint as

$$D_j = \begin{cases} 0 & g_j(\mathbf{d}_s, \mathbf{d}_c) \leqslant g_j^u(\mathbf{d}_s, \mathbf{d}_c), \\ \left(g_j(\mathbf{d}_s, \mathbf{d}_c) - g_j^u(\mathbf{d}_s, \mathbf{d}_c)\right) \Big/ g_j^u(\mathbf{d}_s, \mathbf{d}_c) & \text{otherwise}, \end{cases} \tag{35}$$

where $g_j(\mathbf{d}_s, \mathbf{d}_c)$ and $g_j^u(\mathbf{d}_s, \mathbf{d}_c)$ are the jth constraint function and its corresponding upper bound, respectively.

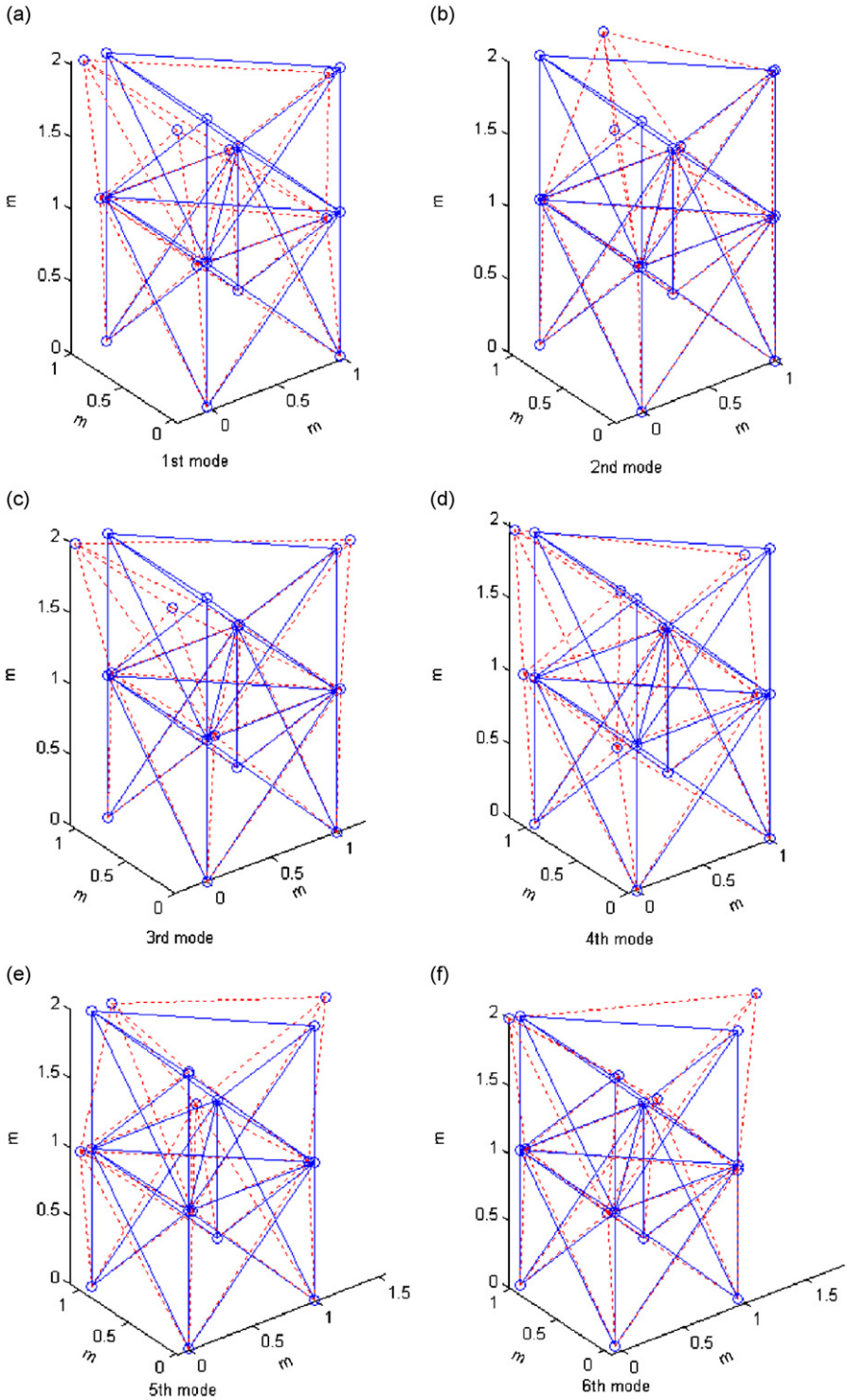

Fig. 16. The controlled mode shapes for case 2 of Condition 1: (a) 1st mode; (b) 2nd mode; (c) 3rd mode; (d) 4th mode; (e) 5th mode; (f) 6th mode.

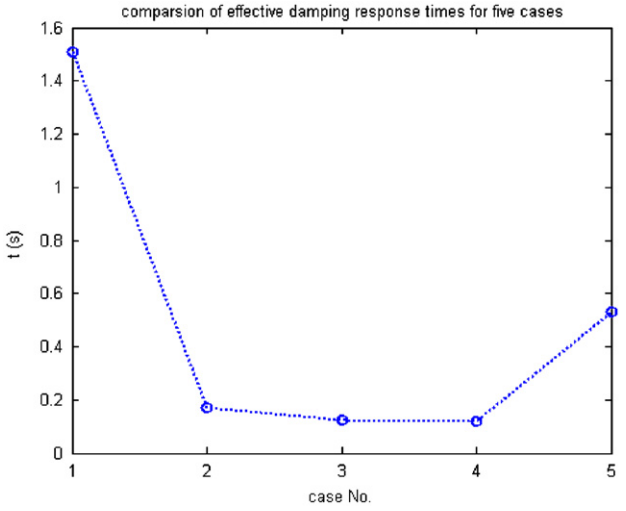

Fig. 17. Comparison of the effective damping response times for five cases of Condition 1.

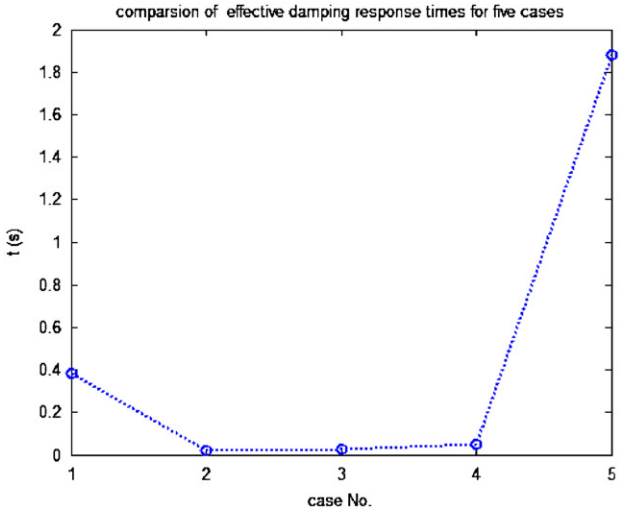

Fig. 18. Comparison of the effective damping response times for five cases of Condition 2.

Then, the fitness for minimizing the objective function and maximizing the objective function can be described, respectively, as

$$\mathrm{eval}(\mathbf{d}_s, \mathbf{d}_c) = 1 \Big/ \left[J(\mathbf{d}_s, \mathbf{d}_c) * \left(1 + \mathrm{penal} * \left(\sum_{j=1}^{p} D_j \right) \Big/ p \right) \right], \tag{36}$$

$$\mathrm{eval}(\mathbf{d}_s, \mathbf{d}_c) = J(\mathbf{d}_s, \mathbf{d}_c) \Big/ \left(1 + \mathrm{penal} * \left(\sum_{j=1}^{p} D_j \right) \Big/ p \right), \tag{37}$$

where p is the number of the constraint functions. 'penal' is the penalty index factor.

Furthermore, taking the cost of actuators into account, the individual fitness is rewritten as

$$\mathrm{eval}'(\mathbf{d}_s, \mathbf{d}_c) = \mathrm{eval}(\mathbf{d}_s, \mathbf{d}_c)/(n_a)^{p_1}, \tag{38}$$

where p_1 is a predetermined value.

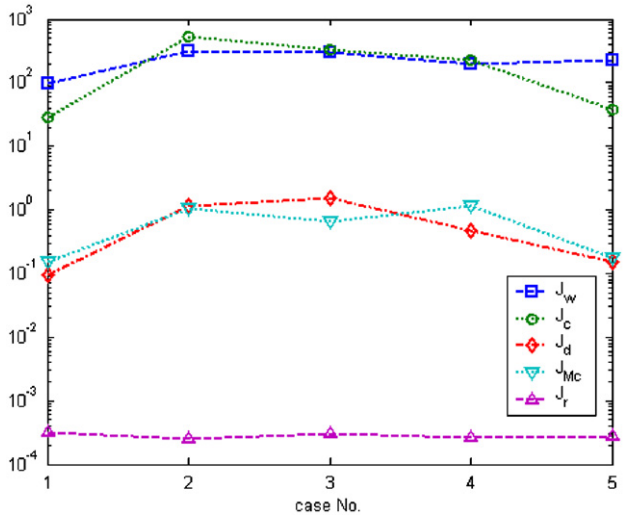

Fig. 19. Curve of comparison of objective functions for five cases of Condition 1.

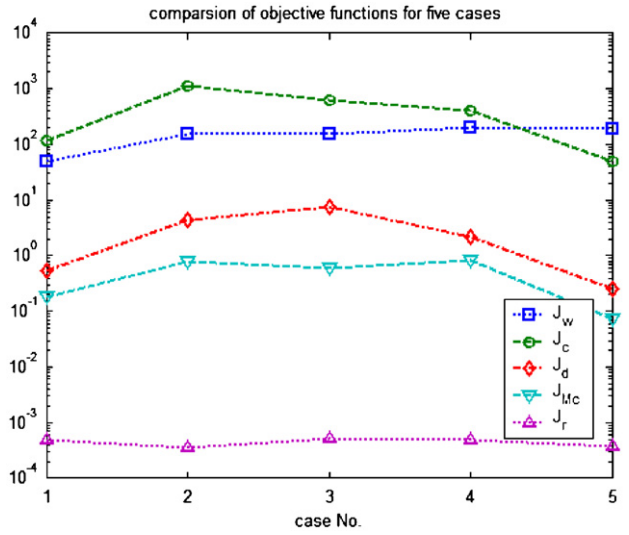

Fig. 20. Curve of comparison of objective functions for five cases of Condition 2.

Similarly, if taking the number of controlled modes into consideration, the individual fitness can be rewritten as

$$\text{eval}'(\mathbf{d}_s, \mathbf{d}_c) = \text{eval}(\mathbf{d}_s, \mathbf{d}_c) * (n_m)^{p_2}, \tag{39}$$

where p_2 is also a predetermined value.

6. *Termination criterion*: The optimization algorithm process is repeated again until the termination criterion is satisfied. The termination criterion could be expressed as

$$\begin{cases} |J^{t+b} - J^t| / J^t \leqslant \varepsilon_2, & b = 1, 2, \ldots, t_0, \\ g_j(\mathbf{d}_s, \mathbf{d}_c) \leqslant g_j^u(\mathbf{d}_s, \mathbf{d}_c), & j = 1, 2, \ldots, p, \end{cases} \tag{40}$$

where J^t and J^{t+b} denote the objective values of the evolutionary generation t and $t+b$, respectively; ε_2 and t_0 are a prescribed small value and the prescribed number, respectively.

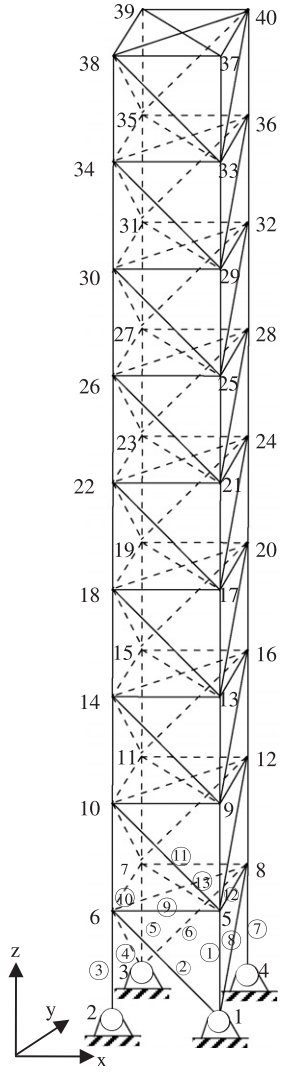

Fig. 21. 126-bar space smart truss.

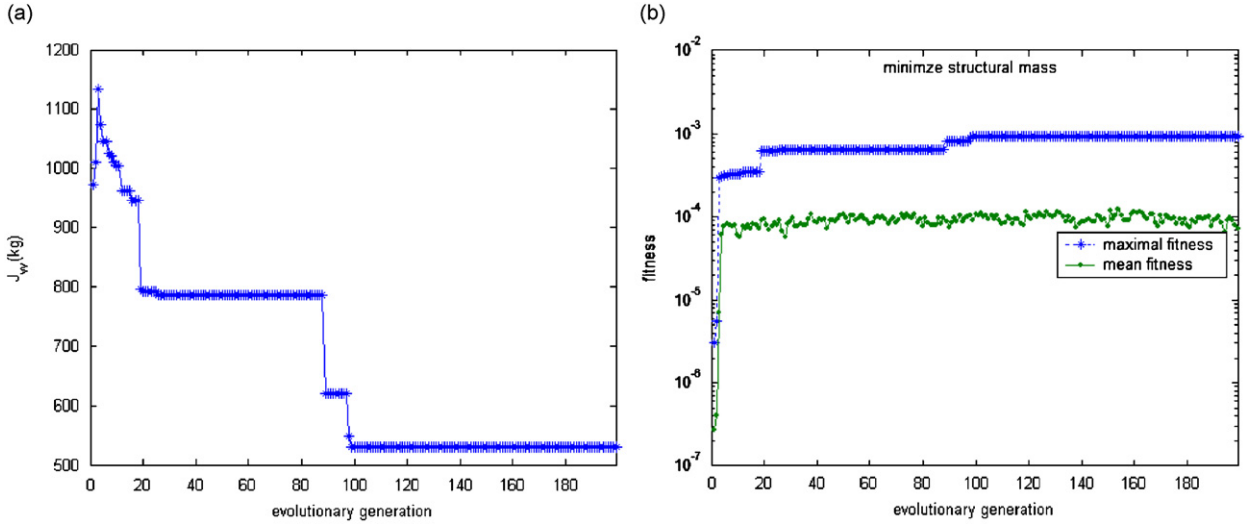

Fig. 22. (a) Curve of structural mass w.r.t. evolutionary generation; (b) curves of the maximal fitness and the mean fitness w.r.t. evolutionary generation.

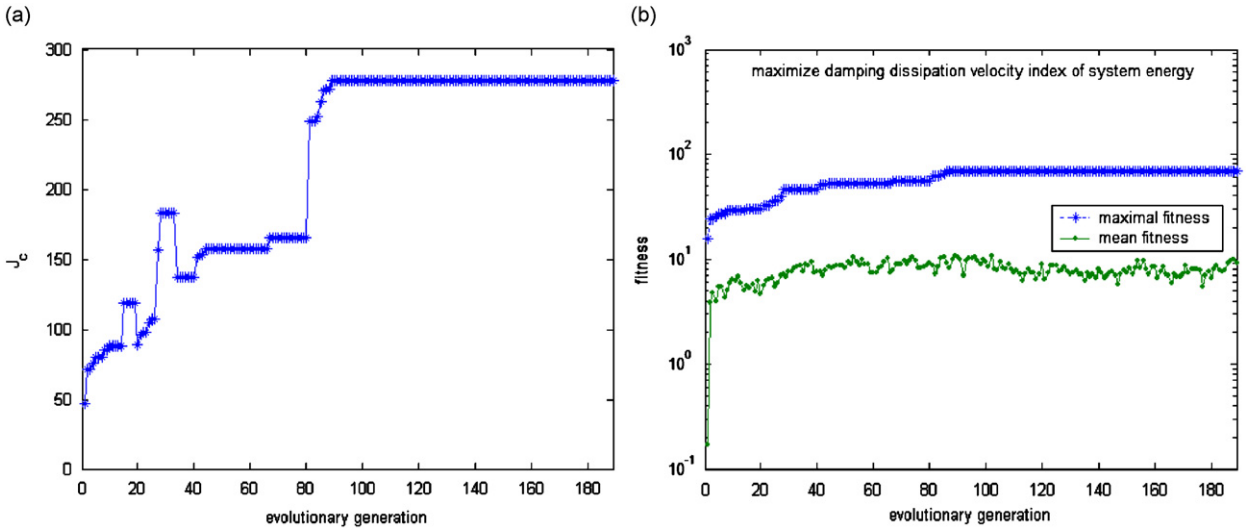

Fig. 23. (a) Curve of the damping dissipation velocity index of system energy w.r.t. evolutionary generation; (b) curves of the maximal fitness and the mean fitness w.r.t. evolutionary generation.

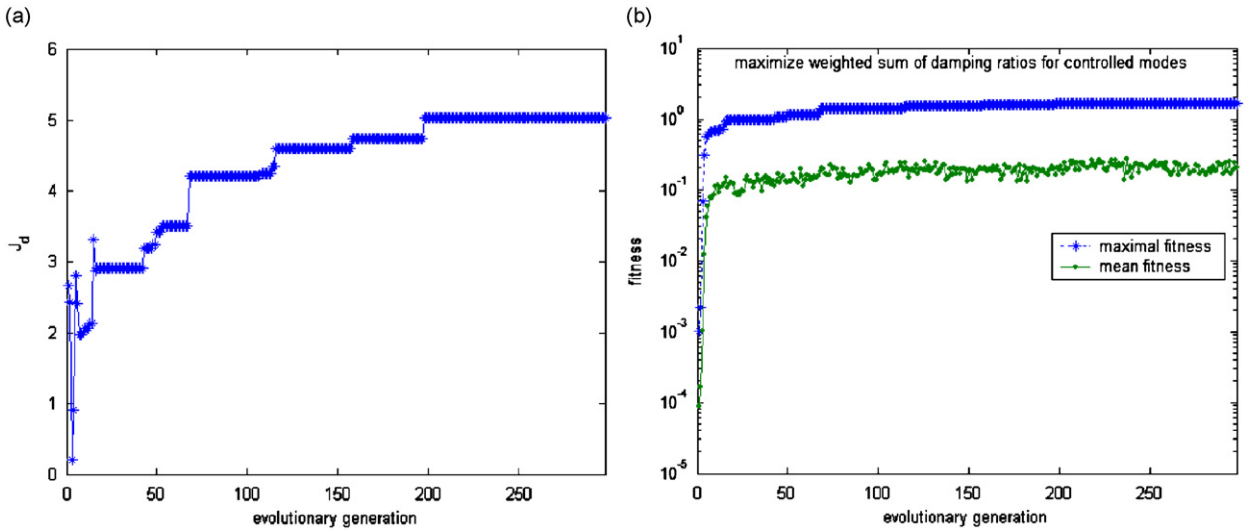

Fig. 24. (a) Curve of the weighted sum of damping ratios for controlled modes w.r.t. evolutionary generation; (b) curves of the maximal fitness and the mean fitness w.r.t. evolutionary generation.

4. Numerical examples

In this section, the integrated optimizations of structural topology and control for a 36-bar and a 126-bar space smart truss are studied, as shown in Figs. 3 and 21, respectively. A piezoelectric active element is commonly composed of piezoelectric stack and two metallic connected bars whose lengths are assumed to be same [19]. Some parameters of the controlled structures are shown in Table 1. The amplitude of applied voltages is not more than 150 V. The definition domain of cross-sectional areas of common truss elements is

$$S = \{80\ \ 125\ \ 180\ \ 259.2\ \ 320\ \ 405\ \ 500\ \ 672.2\ \ 793.8\ \ 1125\ \ 1280\ \ 1620\ \ 2000\ \ 2420\ \ 3125\}\,\mathrm{mm}^2.$$

The stress constraint demands that the maximal value for all members is not greater than 173.2 MPa.

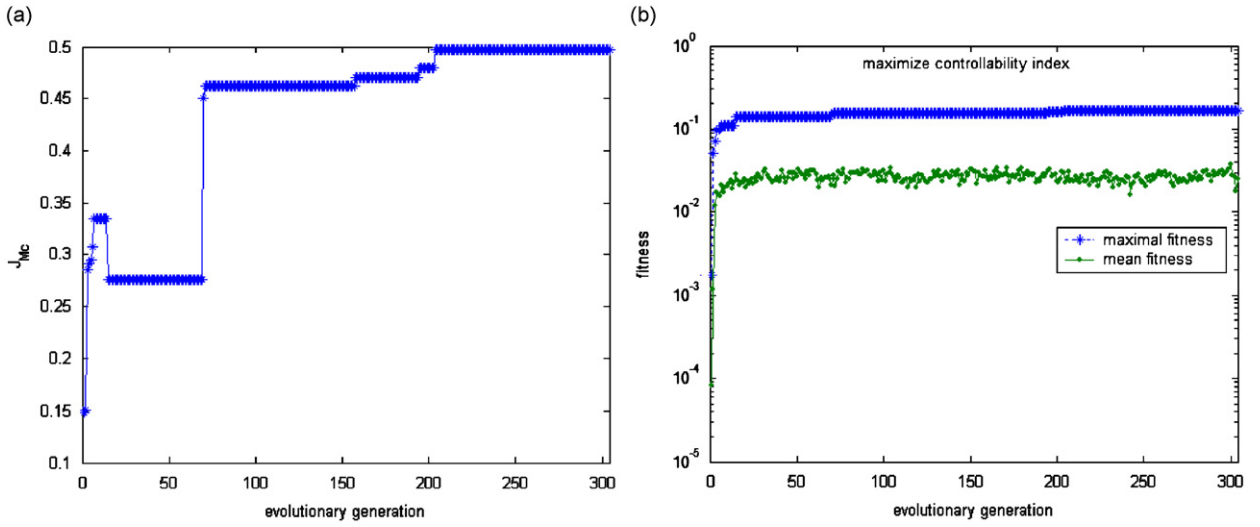

Fig. 25. (a) Curve of controllability index w.r.t. evolutionary generation; (b) curves of the maximal fitness and the mean fitness w.r.t. evolutionary generation.

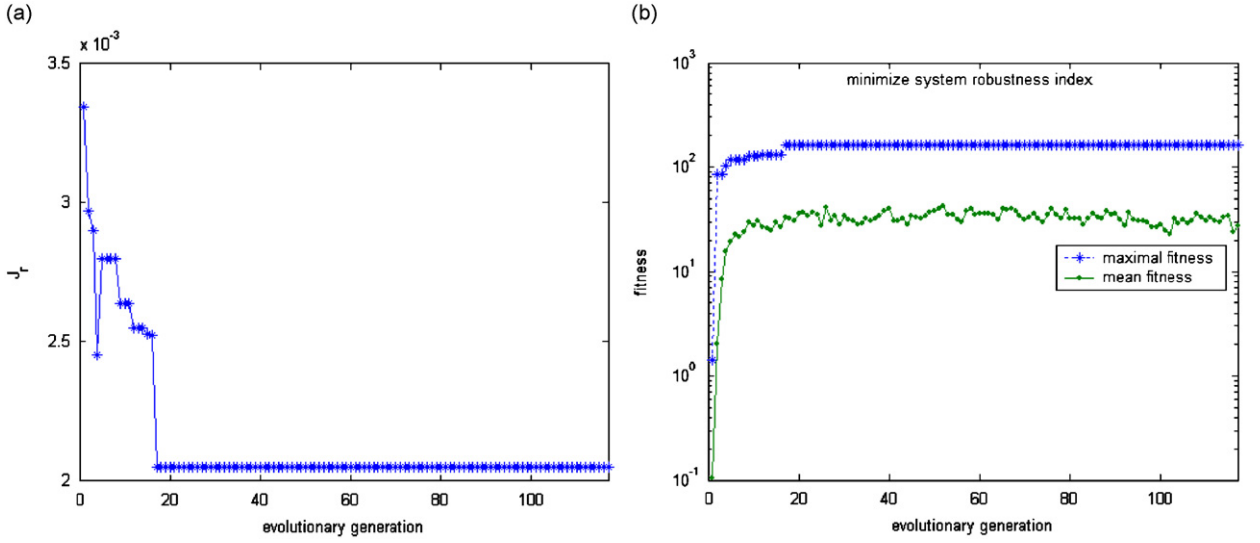

Fig. 26. (a) Curve of system robustness index w.r.t. evolutionary generation; (b) curves of the maximal fitness and the mean fitness w.r.t. evolutionary generation.

In numerical examples, $\varepsilon_1 = 10^{-20}$, penal = 100–1000, $p_1 = p_2 = 1$, $\varepsilon_2 = 1 \times 10^{-4}$ and $t_0 = 100$. Certainly, in order to further strength the effect of the number of assigned actuators or the number of the controlled modes, we can let p_1 and p_2 take the larger value.

4.1. 36-bar space smart truss

The initial disturbance is assumed to be the same as the displacement caused by the applied load of 10,000 N acting in the y-direction of node 12. The static load condition is that a load of 20,000 N is imposed in the y-direction of node 12. The population size, the crossover rate and the mutation rate are 400, 0.8 and 0.02, respectively.

Condition 1: The number of possible assigned actuators is not more than five to control the first six lower modes.

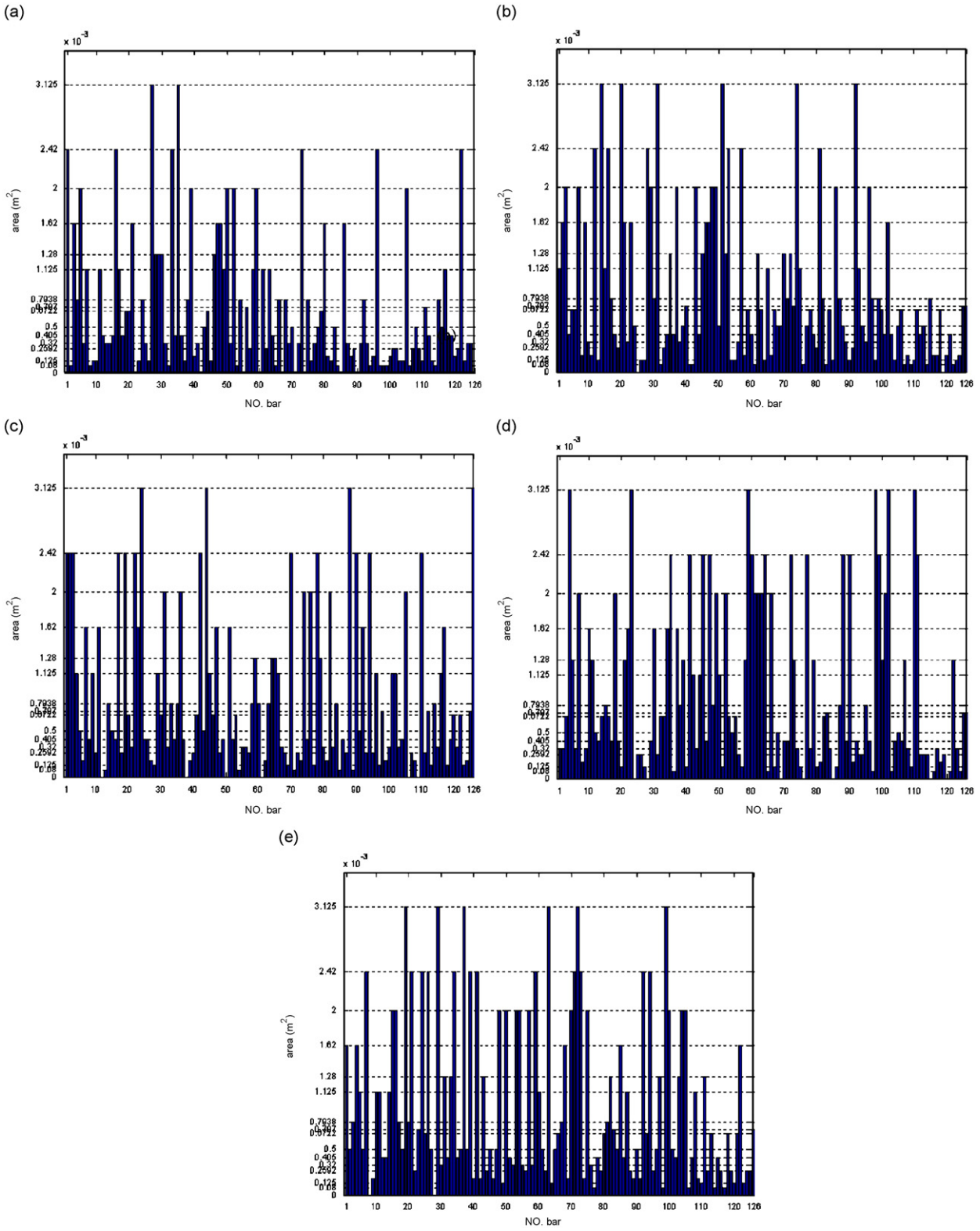

Fig. 27. Optimal cross-section areas for Condition 1: (a) minimizing structural mass; (b) maximizing the damping dissipation velocity index of system energy; (c) maximizing the weighted sum of damping ratios for controlled modes; (d) maximizing controllability index; (e) maximizing system robustness index.

Table 7
Optimal control design variables of 126-bar space smart truss for Condition 1

	r_1	r_2	r_3
Case 1	0.0009323	0.0008550	
Case 2	0.0004621	0.0001053	0.0003118
Case 3	0.0001308	0.0009596	0.0003505
Case 4	0.0007820	0.0009974	0.0005948
Case 5	0.0008963	0.0008102	

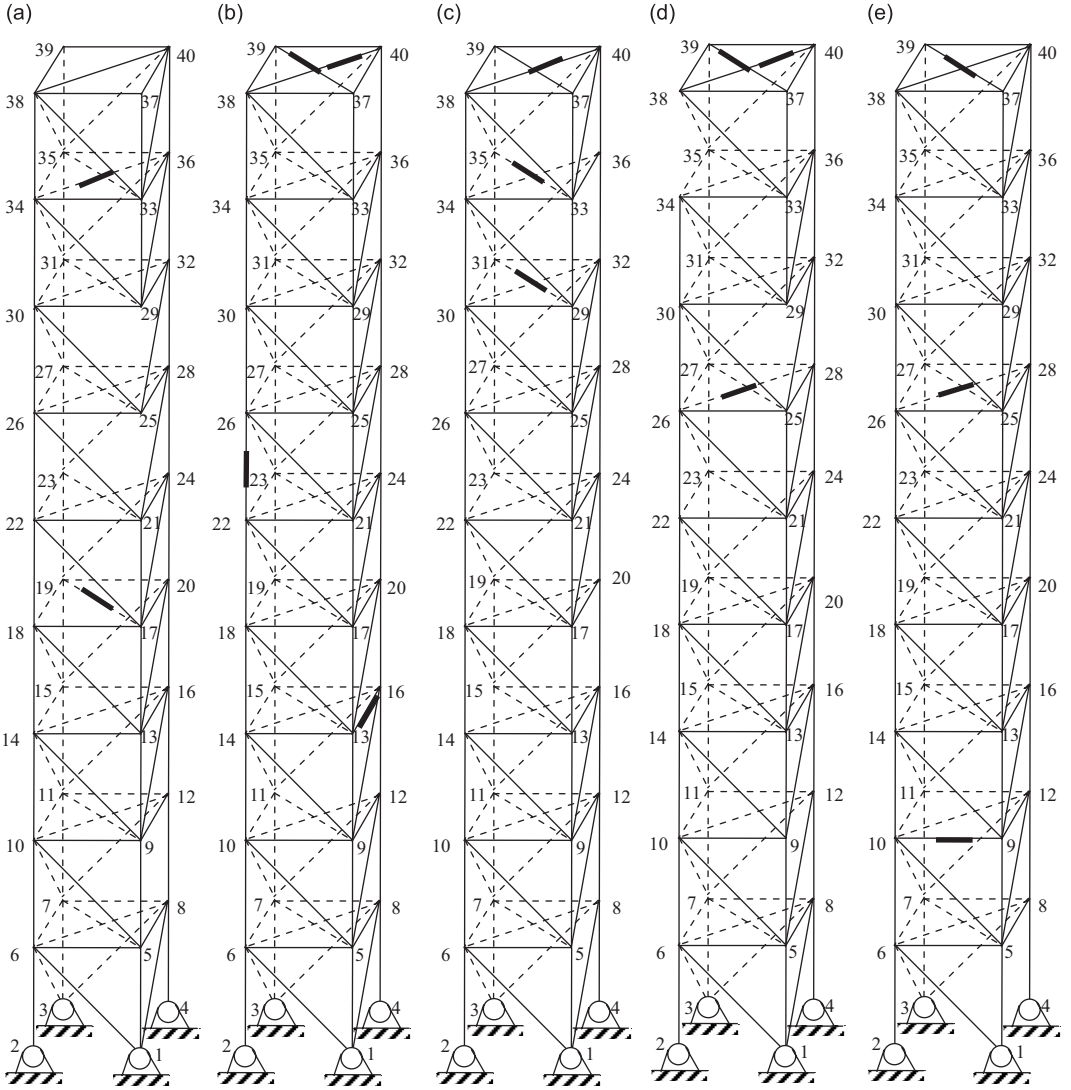

Fig. 28. Optimal topology layouts for Condition 1: (a) minimizing structural mass; (b) maximizing the damping dissipation velocity index of system energy; (c) maximizing the weighted sum of damping ratios for controlled modes; (d) maximizing controllability index; (e) minimizing system robustness index.

The frequency constraint demands that the first frequency of the open-loop system is not less than 100 Hz. The upper and low bounds of each control design variable are 0.001 and 0.0001, respectively. The following five cases are analyzed: (1) minimizing J_W [Structural mass, Eq. (4)]; (2) maximizing J_c [Damping dissipation

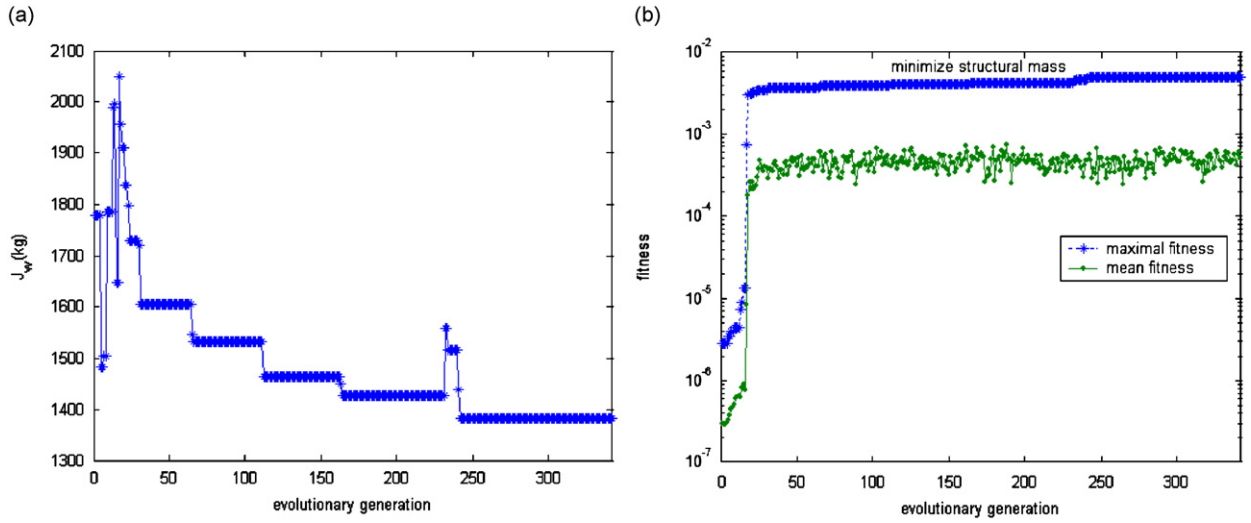

Fig. 29. (a) Curve of structural mass w.r.t. evolutionary generation; (b) curves of the maximal fitness and the mean fitness w.r.t. evolutionary generation.

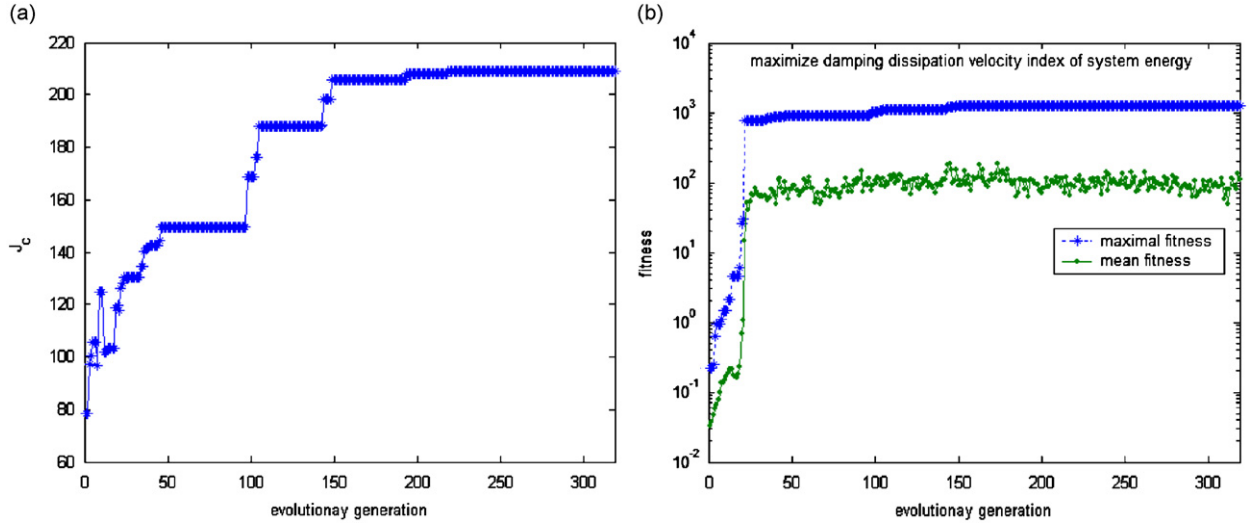

Fig. 30. (a) Curve of the damping dissipation velocity index of system energy w.r.t. evolutionary generation; (b) curves of the maximal fitness and the mean fitness w.r.t. evolutionary generation.

velocity index of system energy, Eq. (11)]; (3) maximizing J_d [Weighted sum of damping ratios for controlled modes, Eq. (15)]; (4) maximizing J_{M_c} [Controllability index, Eq. (19)] and (5) minimizing J_r [System robustness index, Eq. (24)]. For each case, ten optimal solutions of 36-bar space smart truss via random operation are shown in Table 2. It is clear shows that they evolved about ten runs of GA to obtain the best solution.

For five cases, the objective function, the maximal fitness and the mean fitness of the best solution with respect to evolutionary generation are shown in Figs. 4–8, respectively. The optimal characteristics are shown in Table 3. And the optimal design variables, i.e., the cross-sectional areas and the control design variables, are shown in Table 4. The optimal topology layouts of structure and actuator assignment corresponding to five optimization cases are shown in Fig. 9(a)–(e), respectively.

Condition 2: The number of assigned actuators is two to control at least the first three lower modes.

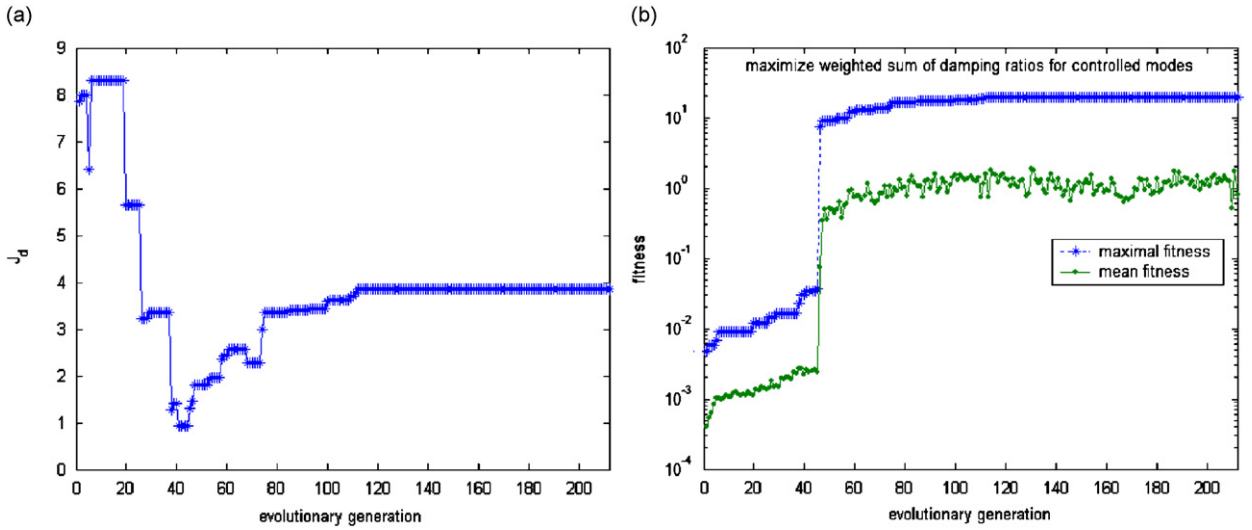

Fig. 31. (a) Curve of the weighted sum of damping ratios for controlled modes w.r.t. evolutionary generation; (b) curves of the maximal fitness and the mean fitness w.r.t. evolutionary generation.

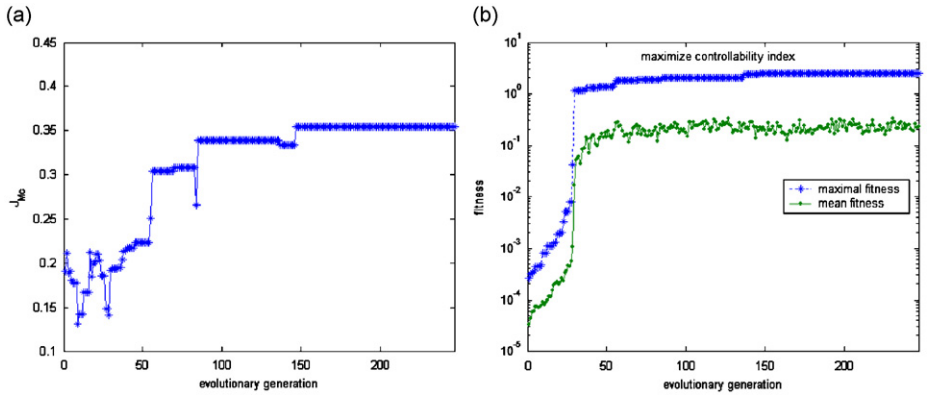

Fig. 32. (a) Curve of controllability index w.r.t. evolutionary generation; (b) curves of the maximal fitness and the mean fitness w.r.t. evolutionary generation.

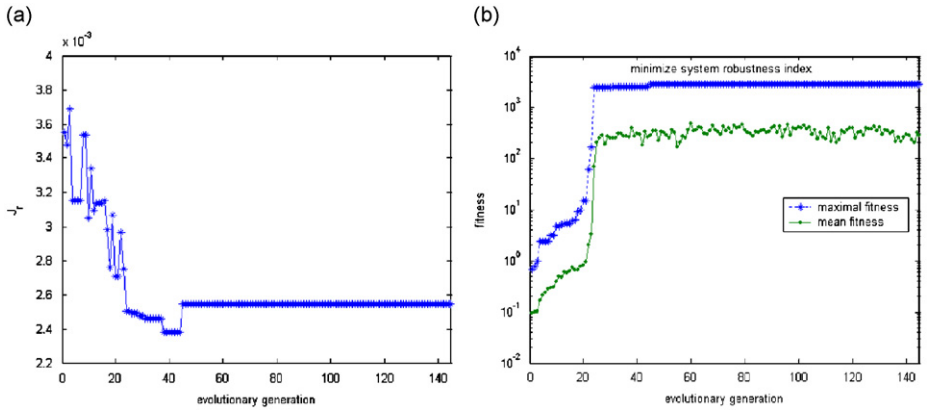

Fig. 33. (a) Curve of system robustness index w.r.t. evolutionary generation; (b) curves of the maximal fitness and the mean fitness w.r.t. evolutionary generation.

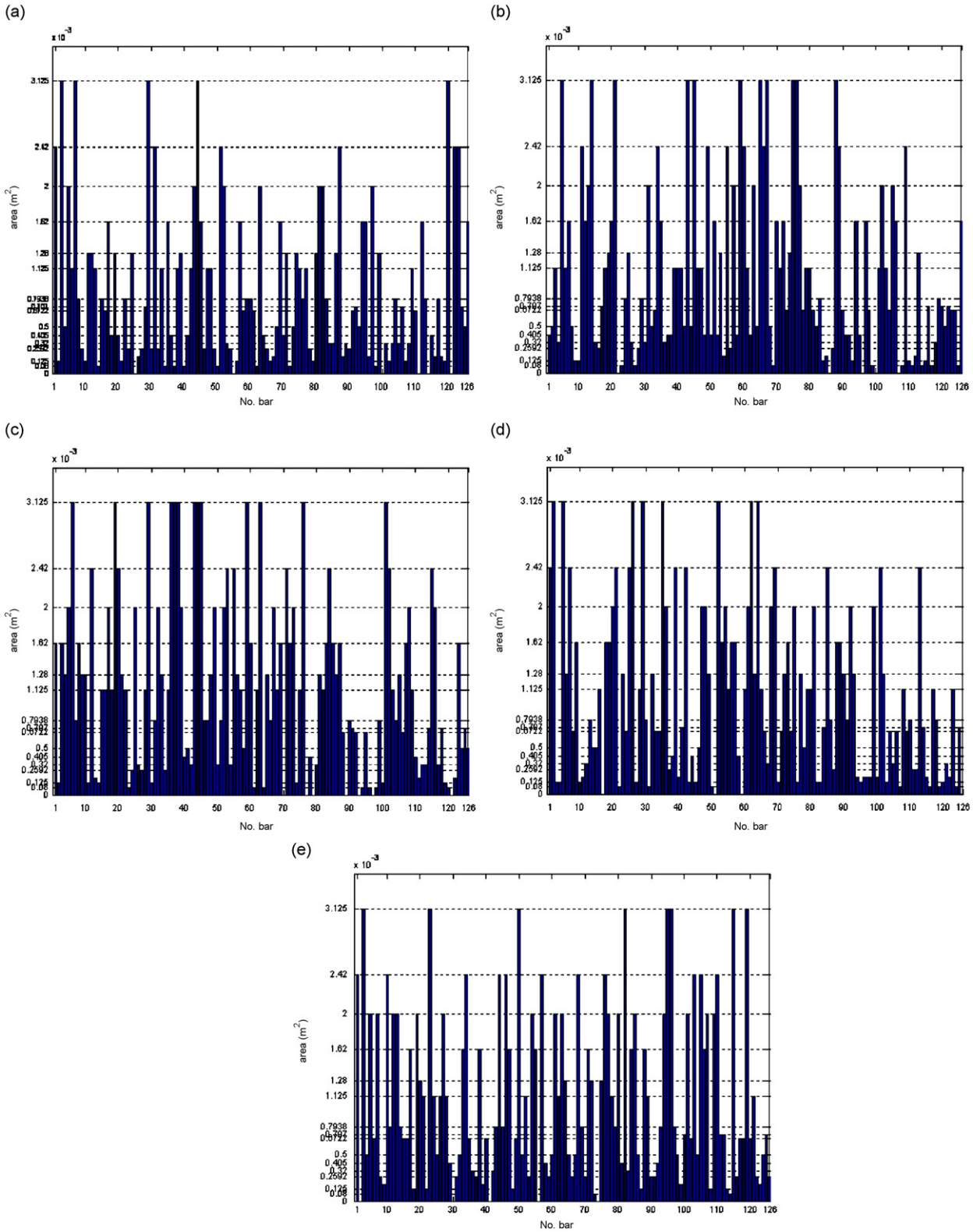

Fig. 34. Optimal cross-section areas for Condition 2: (a) minimizing structural mass; (b) maximizing the damping dissipation velocity index of system energy; (c) maximizing the weighted sum of damping ratios for controlled modes; (d) maximizing controllability index; (e) maximizing system robustness index.

Table 8
Optimal control design variables of 126-bar space smart truss for Condition 2

	r_1	r_2	r_3	r_4
Case 1	0.0001077	0.0001009	0.0001115	0.0000554
Case 2	0.0000825	0.0001183	0.0000902	0.0000806
Case 3	0.0001067	0.0000458	0.0001318	0.0000351
Case 4	0.0001309	0.0000912	0.0001173	0.0001318
Case 5	0.0001106	0.0001067	0.0001086	0.0000757

Table 9
Optimal characteristics of 126-bar space smart truss for Condition 1

	σ_{max} (MPa)	f_1 (Hz)	V_{1max} (V)	V_{2max} (V)	V_{3max} (V)	V_{4max} (V)	Objective function
Case 1	109.97	6.56136	49.8654	110.2699			529.9
Case 2	15.403	7.2076	28.2955	117.3687	3.1189	132.6244	277.5726
Case 3	30.538	5.2671	104.9278	118.2691	141.4735		5.0251
Case 4	18.053	5.1813	97.1622	94.8238	48.0474		0.4976
Case 5	108.31	6.2433	42.5639	124.3182	40.4020		0.0021

Table 10
Optimal characteristics of 126-bar space smart truss for Condition 2

	σ_{max} (MPa)	f_1 (Hz)	V_{1max} (V)	V_{2max} (V)	V_{3max} (V)	V_{4max} (V)	n_m	Objective function
Case 1	134.16	6.9968	70.0433	115.9271	117.9080	132.4287	7	1382.7
Case 2	155.06	7.1694	145.4700	73.3575	120.2764	10.6758	6	209.0031
Case 3	77.020	6.3676	114.3561	136.8932	137.3442	56.0930	5	3.8651
Case 4	138.96	6.0344	133.1907	53.0310	128.6092	94.3538	7	0.3538
Case 5	147.91	6.1428	96.0247	118.7282	113.0254	138.5658	7	0.0025

The upper and low bounds of each control design variable are 0.0001 and 0.00001, respectively. The first natural frequency of the open-loop system must not be less than 80 Hz. Five cases, same as in Condition 1, are analyzed. Subsequently, the optimal solutions including the optimal characteristics and the optimal design variables are shown in Tables 5 and 6, respectively. Also for five cases, the objective function, the maximal fitness and the mean fitness with respect to evolutionary generation are shown in Figs. 10–14, respectively. And the optimal topologies corresponding to five optimization cases, including structural layout and actuator placement, are shown in Fig. 15(a)–(e), respectively.

Some meaningful conclusions can be drawn from these optimal results of Conditions 1 and 2:

(1) For different objective function, the topology layout including structural topology and the optimal assignment of actuators is different. Actuators are always placed in the position where the deformations of the elements are much larger for all controlled modes. For case 2 of Condition 1, the controlled mode shapes are plotted in Fig. 16, the placements of three actuators accord with the fact.
(2) The effective damping response time varies with the objective function. They are respectively 1.5102, 0.1730, 0.1245, 0.1198 and 0.5322 s for five cases of Condition 1, as shown in Fig. 17. And for five cases of Condition 2, they are 0.3858, 0.0206, 0.0278, 0.0492 and 1.8778 s, respectively, as shown in Fig. 18. This shows that the effective damping response time is lowest using the controllability index and the damping dissipation velocity index as the objective functions for Condition 1 and Condition 2, respectively. To minimize structural mass and system robustness index are at the cost of increasing the effective damping response time for both conditions. In some degree, the controllability index, the damping dissipation velocity index and the weighted sum of damping ratios for controlled modes are equivalent for decreasing

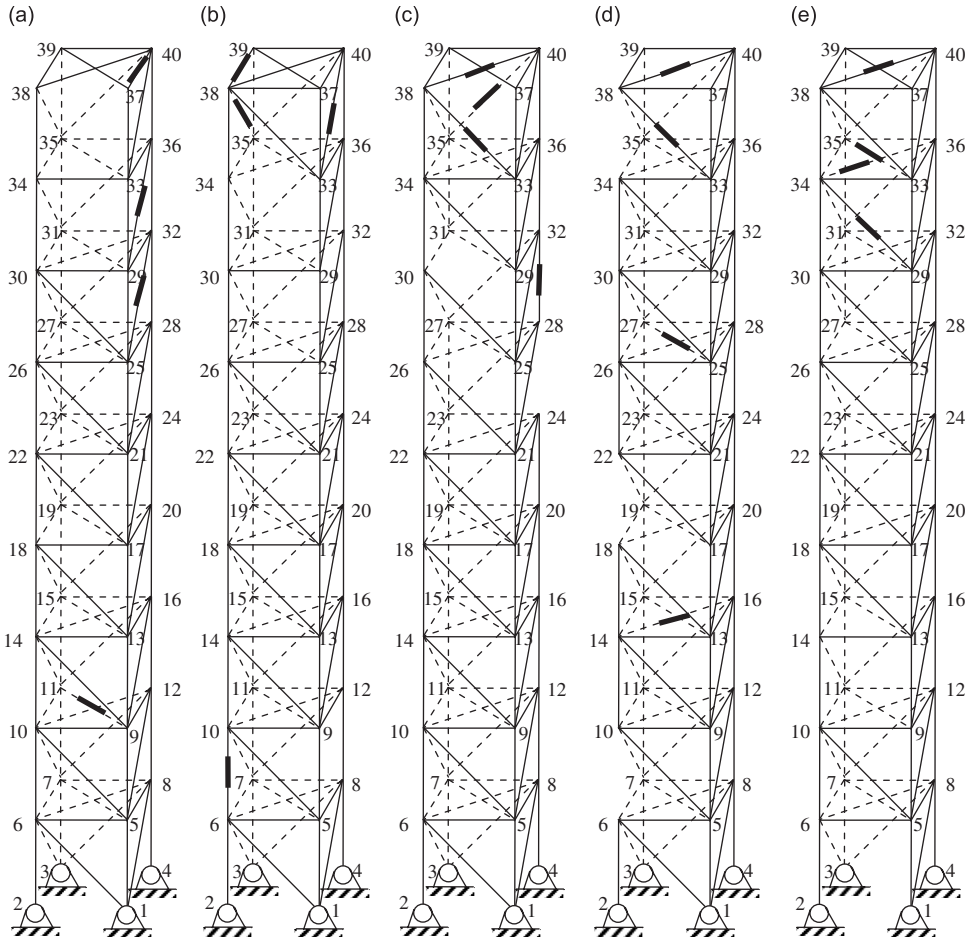

Fig. 35. Optimal topology layouts for Condition 2: (a) minimizing structural mass; (b) maximizing the damping dissipation velocity index of system energy; (c) maximizing the weighted sum of damping ratios for controlled modes; (d) maximizing controllability index; (e) minimizing system robustness index.

the effective damping response time. In essence, these three objective functions are to enlarge the damping ratios of the closed-loop system.

(3) Seen from Figs. 19 and 20, it is impossible to minimize the objective function for five cases of Condition 1 or 2.

(4) There is a difference between the maximal fitness and the mean fitness. This is mainly due to some meaningless individuals in a population.

4.2. 126-bar space smart truss

The static load condition is that a load of 10,000 N is imposed in the y-direction of node 40. The initial disturbance vector is assumed to be the same as the displacement caused by the applied load of 1000 N acting in the y-direction of node 40. The population size, the crossover rate and the mutation rate are 200, 0.8 and 0.02, respectively. The frequency constraint demands that the first natural frequency of the open-loop system is not less than 5 Hz (Fig. 21).

Two conditions are also analyzed as follows:

Condition 1: The permittable maximal number of assigned actuators is five to control the first six lower modes.

The upper and low bounds of each control design variable are 0.001 and 0.0001, respectively. The curves of the objective functions, the maximal fitness and the mean fitness w.r.t. evolutionary generation for five cases, are shown in Figs. 22–26, respectively. The corresponding optimal cross-section areas and the control design variables are list in Fig. 27 and Table 7, respectively. These optimal topologies corresponding to five cases are shown in Fig. 28 and the optimal characteristics are list in Table 9.

Condition 2: The number of assigned actuators is four to control at least the first five lower modes.

The upper and low bounds of each control design variable are 0.0001 and 0.00001, respectively. Some optimal solutions, including the curves of the objective functions, the maximal fitness and the mean fitness w.r.t. evolutionary generation, the optimal cross-section areas and the control design variables are respectively shown in Figs. 29–34 and Table 8, respectively. These optimal characteristics and topologies for five cases are respectively shown in Table 10 and Fig. 28.

Certainly, the conclusions for 36-bar space smart truss can also be appropriate for the optimal solutions of 126-bar space smart truss (Fig. 35).

5. Conclusions

In order to suppress structural vibration more efficiently, the optimal model proposed integrates the dynamic optimization with considerations of the aspects of structure and control. Structural topology and the number of actuators/the number of controlled modes are also taken as design variables. A new optimization strategy based on GA is put forward to deal with the integrated optimization of structural topology and control for piezoelectric smart trusses. It is obvious that the optimal topology layout varies with the objective function. Actuators are often placed in the position where the deformations of the elements are much larger for all controlled modes. Maximizing the damping dissipation velocity index, the controllability index and the weighted sum of damping ratios are more efficient than optimizing other objective functions for the effective damping response time. Certainly, how to put forward the suited objective function and the multiobjective optimization about this topic are also our further research emphases.

Acknowledgments

The authors would like to thank for the support by Natural Science Foundation of China under Grant 10472093 and the Doctorate Creation Foundation of Northwestern Polytechnical University under Grant 200236.

Appendix A. Coupled modal space control

It is assumed that the structural damping is neglected in the paper because it is very small commonly for the metal truss structure and the control effect predicted for the case without damping is conservative one which is safer for the engineering practice. The dynamic behavior for the smart truss under initial disturbance is then determined by the equations:

$$\begin{cases} \mathbf{M}\ddot{\mathbf{x}}(t) + \mathbf{K}\mathbf{x}(t) = \mathbf{B}\mathbf{u}(t), \\ \mathbf{x}(0) = \mathbf{x}_0 \quad \dot{\mathbf{x}}(0) = \dot{\mathbf{x}}_0, \end{cases} \tag{A.1}$$

where $\mathbf{x}(t) \in R^n$ and $\ddot{\mathbf{x}}(t) \in R^n$ are the system nodal displacement and acceleration vectors, respectively, and n is the number of the degrees of freedom of the controlled system; $\mathbf{M}$ and $\mathbf{K}$ are the mass matrix and the stiffness matrix, respectively; $\mathbf{B}$ is the actuator distributing matrix and the corresponding feasible domain is $\Omega : \mathbf{B}_{n\times n_a}$, where the element of $\mathbf{B}_{n\times n_a}$ is 0 or 1 and n_a is the number of assigned actuators; $\mathbf{u}(t) \in R^{n_a}$ is the control force vector; $\mathbf{x}_0$ and $\dot{\mathbf{x}}_0$ are the initial displacement and velocity disturbances, respectively.

By coordinate transformation, Eq. (A.1) can be changed into the following modal form:

$$\begin{Bmatrix} \ddot{\mathbf{y}}_c(t) \\ \ddot{\mathbf{y}}_r(t) \end{Bmatrix} + \begin{bmatrix} \mathbf{\Lambda}_c & 0 \\ 0 & \mathbf{\Lambda}_r \end{bmatrix} \begin{Bmatrix} \mathbf{y}_c(t) \\ \mathbf{y}_r(t) \end{Bmatrix} = \begin{Bmatrix} \boldsymbol{\varphi}_c^{\mathrm{T}} \\ \boldsymbol{\varphi}_r^{\mathrm{T}} \end{Bmatrix} \mathbf{B}\mathbf{u}(t), \tag{A.2}$$

where $\mathbf{y}_c(t) \in R^{n_m}$ and $\ddot{\mathbf{y}}_c(t) \in R^{n_m}$ are the modal displacement and the modal acceleration vectors of the controlled modes, respectively; $\boldsymbol{\varphi}_c = \begin{bmatrix} \boldsymbol{\varphi}_1 & \cdots & \boldsymbol{\varphi}_{n_m} \end{bmatrix}$ and n_m is the number of the controlled modes; the diagonal eigenvalue matrix $\boldsymbol{\Lambda}_c$ is explained as $\mathrm{diag}(\omega_1^2, \omega_2^2, \cdots, \omega_{n_m}^2) \in R^{n_m \times n_m}$, where $\omega_i (i = 1, 2, \ldots, n_m)$ is the ith-order natural frequency. Similarly, the subscript r is associated with the uncontrolled modes.

The state-space equations of controlled modes corresponding to Eq. (A.2) can be expressed as

$$\dot{\mathbf{Z}}(t) = \mathbf{A}\mathbf{Z}(t) + \mathbf{B}'\mathbf{u}(t), \tag{A.3}$$

where

$$\mathbf{Z}(t) = \begin{bmatrix} \mathbf{y}_c(t) \\ \dot{\mathbf{y}}_c(t) \end{bmatrix}, \quad \mathbf{A} = \begin{bmatrix} \mathbf{0}_{n_m \times n_m} & \mathbf{I}_{n_m \times n_m} \\ -\boldsymbol{\Lambda}_c & \mathbf{0}_{n_m \times n_m} \end{bmatrix}, \quad \mathbf{B}' = \begin{bmatrix} \mathbf{0}_{n_m \times n_a} \\ \boldsymbol{\varphi}_c^{\mathrm{T}}\mathbf{B} \end{bmatrix}. \tag{A.4}$$

Assuming that the modal displacements and velocities of the controlled modes can be observed by sensors, in order to guarantee the controllability of the system, the actuators' placements must satisfy the following condition:

$$\mathrm{rank}[\mathbf{B}' \quad \mathbf{A}\mathbf{B}' \quad \mathbf{A}^2\mathbf{B}' \cdots \mathbf{A}^{2n_m-1}\mathbf{B}'] = 2n_m. \tag{A.5}$$

The quadratic objective function introduced is

$$J = \frac{1}{2}\int_0^\infty \left(\mathbf{Z}^{\mathrm{T}}(t)\mathbf{Q}\mathbf{Z}(t) + \mathbf{u}^{\mathrm{T}}(t)\mathbf{R}\mathbf{u}(t)\right) \mathrm{d}t, \tag{A.6}$$

where $\mathbf{Q}$ is a positive semi-definite matrix, and $\mathbf{R}$ is a positive definite weighting matrix. It can be shown that $\mathbf{R} = \mathrm{diag}(r_1, r_2, \ldots, r_{n_a})$ is a diagonal matrix for the control force vector. Assuming

$$\mathbf{Q} = \begin{bmatrix} \boldsymbol{\Lambda}_c & \mathbf{0}_{n_m \times n_m} \\ \mathbf{0}_{n_m \times n_m} & \mathbf{I}_{n_m \times n_m} \end{bmatrix},$$

J can be regarded as the sum of the modal potential energy and the modal kinetic energy of the controlled system as well as the performance index of input energy for the required control forces.

The minimization of Eq. (A.6) results in

$$\mathbf{u}(t) = -\mathbf{R}^{-1}\mathbf{B}'^{\mathrm{T}}\mathbf{P}\mathbf{Z}(t), \tag{A.7}$$

where $\mathbf{P} \in R^{2n_m \times 2n_m}$ is the positive semidefinite symmetric matrix, and satisfies the following Riccati equation:

$$\mathbf{P}\mathbf{A} + \mathbf{A}^{\mathrm{T}}\mathbf{P} + \mathbf{Q} - \mathbf{P}\mathbf{B}'\mathbf{R}^{-1}\mathbf{B}'^{\mathrm{T}}\mathbf{P} = \mathbf{0}. \tag{A.8}$$

Substituting Eq. (A.7) into Eq. (A.3), the state equation for the closed-loop system can be expressed as

$$\dot{\mathbf{Z}}(t) = \bar{\mathbf{A}}\,\mathbf{Z}(t), \tag{A.9}$$

where $\bar{\mathbf{A}} = \mathbf{A} - \mathbf{B}'\mathbf{R}^{-1}\mathbf{B}'^{\mathrm{T}}\mathbf{P}$.

Then the effective damping response time for the coupled modal space control [19] is

$$t_e = \frac{\mathbf{Z}^{\mathrm{T}}(0)\mathbf{Q}\mathbf{Z}(0)}{\mathbf{Z}^{\mathrm{T}}(0)\mathbf{P}\mathbf{Z}(0)}. \tag{A.10}$$

References

[1] B. Xu, J.S. Jiang, W.H. Tong, K.G. Wu, Topology group concept for truss topology optimization with frequency constraints, *Journal of Sound and Vibration* 261 (2003) 911–925.

[2] N.L. Pedersen, A.K. Nielsen, Optimization of practical trusses with constraints on eigenfrequencies, displacements, stresses, and buckling, *Structural Optimization* 23 (2003) 436–455.

[3] C.S. Jog, Topology design of structures subjected to periodic loading, *Journal of Sound and Vibration* 253 (3) (2002) 687–709.

[4] T.S. Kim, J.E. Kim, Y.Y. Kim, Parallelized structural topology optimization for eigenvalue problems, *International Journal of Solids and Structures* 41 (2004) 2623–2641.

[5] H. Guan, Y.J. Chen, Y.C. Loo, Y.M. Xie, G.P. Steven, Bridge topology optimization with stress, displacement and frequency constraints, *Computers and Structures* 81 (2003) 131–145.
[6] D. Thakkar, R. Ganguli, Helicopter vibration reduction in forward flight with induced shear based piezoceramic actuation, *Smart Materials and Structures* 30 (3) (2004) 599–608.
[7] P. Gardonio, E. Bianchi, S.J. Elliott, Smart panel with multiple decentralized units for the control of sound transmission—part I: theoretical predictions, *Journal of Sound and Vibration* 274 (2004) 163–192.
[8] L. Edery-Azulay, H. Abramovich, Active damping of piezo-composite beams, *Composite Structures* 74 (2006) 458–466.
[9] S.-B. Choi, Active structural acoustic control of a smart plate featuring piezoelectric actuators, *Journal of sound and vibration* 294 (2006) 421–429.
[10] W. Gao, Stochastically optimal active control of a smart truss structure under stationary random excitation, *Journal of Sound and Vibration* 290 (3–5) (2006) 1256–1268.
[11] G. Song, V. Sethib, H.-N. Lic, Vibration control of civil structures using piezoceramic smart materials: a review, *Engineering Structures* 28 (2006) 1513–1524.
[12] C.M.A. Vasques, J. Dias Rodrigues, Active vibration control of smart piezoelectric beams: Comparison of classical and optimal feedback control strategies, *Computers and Structures* 84 (22–23) (2006) 1402–1414.
[13] Z.D. Wang, S.H. Chen, W.Z. Han, Integrated structural and control optimization of intelligent structures, *Engineering Structures* 21 (1999) 183–191.
[14] I.M. Fonseca, P.M. Bainum, M.C. Santos, CPU time consideration for LSS structural/control optimization models with different degrees of freedom, *Acta Astronautica* 54 (2004) 259–266.
[15] X.J. Liu, D.W. Begg, On simultaneous optimisation of small structures—part I: theory, *Computer Methods in Applied Mechanics and Engineering* 184 (2000) 15–24.
[16] X.J. Liu, D.W. Begg, On simultaneous optimisation of small structures—part II: algorithms and examples, *Computer Methods in Applied Mechanics and Engineering* 184 (2000) 25–37.
[17] K.S. Park, H.M. Koh, Preference-based optimum design of an integrated structural and control using genetic algorithms, *Advances in Engineering Software* 35 (2) (2004) 85–94.
[18] Y. Zhu, J. Qiu, H. Du, J. Tani, Simultaneous optimal design of structural topology, actuator locations and control parameters for a plate structure, *Computational Mechanics* 29 (2002) 89–97.
[19] B. Xu, J.S. Jiang, Integrated optimization of structure and control for piezoelectric intelligent trusses with uncertain placement of actuators and sensors, *Computational Mechanics* 33 (2004) 406–412.